Multi-scale modeling of microplastics transport in marine environments

THISAL MANDULA SUGATHAPALA

Department of Mechanics and Maritime Sciences Chalmers University of Technology Gothenburg, Sweden, 2025

Multi-scale modeling of microplastics transport in marine environments

THISAL MANDULA SUGATHAPALA

Acknowledgements, dedications, and similar personal statements in this thesis, reflect the author's own views.

© Thisal Mandula Sugathapala 2025 except where otherwise stated.

Department of Mechanics and Maritime Sciences Chalmers University of Technology SE-412 96 Gothenburg, Sweden

Phone: +46 (0)31 772 1000

Printed by Chalmers Digital Printing Gothenburg, Sweden, June 2025

Multi-scale modeling of microplastics transport in marine environments

THISAL MANDULA SUGATHAPALA
Department of Mechanics and Maritime Sciences
Chalmers University of Technology

Abstract

Over the past seventy years, plastic has thrived across numerous industries thanks to its low cost and exceptional properties. Yet, those very qualities make plastic pollution a significant environmental concern. Microplastics refer to plastic particles of sizes between 1 μm and 1 mm. Due to their small sizes, once microplastics enter marine environments, they become essentially irretrievable. Hence, there is a growing urgency to assess the ecological impact of microplastic pollution. Numerical tools are widely used to enhance our understanding of the ocean's state and its influence on microplastic transport and fate. However, the challenge is accurately capturing the wide range of scales involved, which can range from μm to km. To address this issue, a multiscale modeling framework is presented. At the "small scale," direct numerical simulations are performed to resolve particles settling in turbulent marine environments and extract relevant correlations. These correlations are tested for suitability when scaling up, at an "intermediate scale", with controlled environmental conditions. Finally, numerical results from large-scale simulations, combined with field observations, are used to identify the dominant mechanisms in marine environments that govern the transport and ultimate fate of microplastics. The proposed approach extends the capabilities of numerical models beyond mere predictive tools, providing a robust foundation for conducting environmental impact assessments.

Keywords: Multi-scale models, Microplastics, Direct numerical simulations, Lagrangian particle tracking, Plastic pollution, Biofouling, Stratification

"Character beats talent" - Johan Sundstein

List of Publications

This thesis is based on the following publications:

- [A] **Thisal Mandula Sugathapala**, Tonia Capuano, Luca Brandt, Daniele Iudicone, Gaetano Sardina, "Vertical transport of buoyant microplastic particles in the ocean: The role of turbulence and biofouling". *Environmental Pollution*, vol. 369, pp. 125819 (2025).
- [B] **Thisal Mandula Sugathapala**, Rishabh More, Arezoo Ardekani, Luca Brandt, Gaetano Sardina, "Particles settling in turbulent stratified flows: a multiscale approach". *To be submitted to a scientific journal.* (2025).
- [C] **Thisal Mandula Sugathapala**, Martin Hassellöv, Lars Arneborg, Bengt Liljebladh, Karin Mattsson, Amanda T. Nylund, Ida-Maja Hassellöv, Rickard Bensow, Gaetano Sardina, "A numerical framework for microplastics transport in marine environments: A case study of the Orust-Tjörn fjord system". *To be submitted to a scientific journal.* (2025).

Contents

Αŀ	ostrac	t t	i
Lis	st of	Papers	V
Αc	know	vledgements	κi
Αŀ	brev	iations	ii
No	omen	clature x	V
ı	Ex	tended Summary	1
1	Intro	oduction	3
	1.1	Background	4
	1.2		5
	1.3		7
	1.4	Thesis outline	9
	1.5		0
2	Fully	y resolved flows 1	1
	2.1	Stratification	2

D	foror		57
6	Con	cluding Remarks and Future Work	55
	5.3	Large scales	52
	5.2	Intermediate scales	51
	5.1	Micro scales	50
5	A h	olistic approach to modeling marine litter transport	49
		Fate of Polyethylene pellets	47
		Biofouling and sediment transport	
		Microplastic pollution	44
	4.3	Case study: Stenungsund	44
		Sediment transport model	44
		Biofouling	44
		Modified settling velocity	43
		Vertical motion	43
		Horizontal motion	43
	4.2	Numerical framework	
•	4.1	MPDrift	
4	Larg	ge-scale simulations	41
	3.5	Turbulence vs biofouling	37
	3.4	Impact of turbulence on biofouling rate	35
	3.3	LPT numerical setup	
	3.2	Biofouling	32
	3.1	Settling velocity PDF in stratified flows	30
3	Мо	deling intermediate scales	29
	2.7	Theoretical limits for settling velocity (special case)	26
	2.6	Drag enhancement and reduction	24
	2.5	Particles settling in unstable stratified flows (Derivation)	20
	2.4	DNS with Immersed Boundary Method	17
	2.3	Intermittency of density gradient	
	2.2	Pseudo-spectral DNS	
	2.2	Pseudo-spec	tral DNS

11	Pa	pers		67
Α	Biof	ouling		Α1
В	Stra	tificatio	on	В1
	1	Introd	uction	B3
	2	Metho	odology	B5
		2.1	Governing equations	B5
		2.2	Simulation parameters	В8
	3	Result	s and Discussion	B12
		3.1	Intermittency of density gradient in stratified turbulence	B12
		3.2	Drag induced on particles settling in stratified turbulence	eB15
		3.3	Impact of turbulent intermittency on a particle's set-	
			tling velocity	B18
		3.4	Normalized PDFs of Settling Velocity	B20
	4	Conclu	usion	B22
	Refe	rences		B22
С	MPI	Orift		C 1
	1	Introd	uction	C3
	2	Metho	odology	C6
		2.1	Horizontal motion	C6
		2.2	Eddy diffusivity	C7
		2.3	Modified settling velocity	C8
		2.4	Biofouling	C9
		2.5	Sediment transport model	C10
	3	Result	s and Discussion	C12
		3.1	Polyethylene pellets	C12
		3.2	Polyvinylchloride particles	
	4	Conclu	usion	
	Rofo	roncoc		

Acknowledgments

I would like to thank my supervisors, Gaetano Sardina, Ida-Maja Hassellöv, and Rickard Bensow, for providing me with the opportunity to pursue a PhD in a subject that has captured my passion since my bachelor's studies. In Sri Lanka, there is a pressing need for experts in fundamental sciences, particularly in the field of fluid mechanics. This project has not only allowed me to deepen my understanding of its core principles but also to apply them to a practical challenge close to home: plastic pollution. Your patience and unwavering support as I navigated this highly interdisciplinary work have been invaluable. I am proud of how far I have come under your guidance, slowly learning from each of your distinct areas of expertise.

I also extend my gratitude to the many collaborators whose insights and constructive feedback, shared during our meetings and discussions, have greatly improved the quality of this work. To all my coworkers in the division, it has been an absolute pleasure spending time with you. Thank you for making the usual "stressful" PhD life more fun and exciting. A special shout-out to the multi-phase group, our shared lunches and adventures on work trips have been unforgettable.

I would like to extend my deepest gratitude to my family for their unwavering love and support throughout my educational endeavors in Sweden. Finally, I am incredibly grateful to all my friends from home, most of whom have moved to different countries, yet always gather daily on Discord. Your constant presence has been a true comfort, and sharing laughs with you has made me feel anything but alone.

Abbreviations

CTD: Conductivity, Temperature, and Depth profile

DAPSIR: Drivers, Activities, Pressures, State, Impact, Response

DL: Deep Layer

DNS: Direct Numerical Simulations

EU: European Union

FFT: Fast Fourier Transform

HDPE: High Density Polyethylene

IBM: Immersed Boundary Method

LPT: Lagrangian Particle Tracking

LDPE: Low Density Polyethylene

ML: Mixed Layer

MP: Microplastics

MSFD: Marine Strategic Framework Directive

NS: Near Sea Floor

OGCM: Ocean General Circulation Models

PDF: Probability Distribution Function

PP: Polypropylene

TP: Thermocline, Pycnocline

Nomenclature

Greek Letters

ω :	Angular velocity	$\rm rads^{-1}$
β :	Thermal expansion coefficient	K^{-1}
γ :	Density gradient	${\rm kg}{\rm m}^{-4}$
ρ :	Density	${\rm kg}{\rm m}^{-3}$
ν :	Kinematic viscosity	$\mathrm{m}^2\mathrm{s}^{-1}$
μ :	Dynamic viscosity	Pas
κ :	Thermal diffusivity	$\mathrm{m^2s^{-1}}$
ϵ :	Turbulence dissipation rate	$\mathrm{m}^2\mathrm{s}^{-3}$
au:	Shear stress	Pa
θ :	Langmuir circulation factor	_

Roman Letters

A:	Algae concentration	${\rm kgm^{-3}}$
N:	Brunt–Väisälä frequency	s^{-1}
C_d :	Drag coefficient	[-]
<i>g</i> :	Gravitational acceleration	${\rm ms^{-2}}$
f_2 :	IBM forcing term	Pa
d:	Particle diameter	m
<i>P</i> :	Pearson correlation coefficient	[-]

T: Temperature Κ t: Time \mathbf{S} R: Random number [-]S: [-]Skewness Spectral DNS forcing term f_1 : Pa $\rm m\,s^{-1}$ Velocity u: m^3 V: Volume m^{-1} k: Wavenumber

Subscripts and Superscripts

*: Dimensional value

': Fluctuations from infinity

 ρ : Density

0: Reference value

f: Fluid

H: Help points

L: Lagrangian points

p: Particle

t: Temperature

r: Radius

S: Surface points

z: Vertical direction

Part I Extended Summary

CHAPTER 1

Introduction

This thesis presents a multi-scale modeling framework to investigate the transport and fate of microplastics in marine environments. The proposed methodology integrates three core modeling methods: particle and flow-resolving simulations to capture detailed particle settling dynamics, particle tracking models to investigate fundamental mechanisms governing microplastics' motion within controlled scenarios, and large-scale models to explore source-to-sink pathways of microplastics in realistic ocean conditions. For improved scientific understanding, numerical investigations on the fate of microplastics should be carried out across different scales, and the findings should be integrated into a framework for environmental impact assessment. This approach extends the scope of numerical simulations beyond that of predictive tools. Accordingly, this thesis will explore the potential to form a link between numerical simulations used to obtain fundamental knowledge of complex particle-fluid interactions and broader environmental implications. The following chapters provide an overview of the proposed framework, examine each modeling component in detail, and describe their integration across scales. Collectively, they form a comprehensive framework for advancing our understanding of the fate of microplastics in marine environments.

1.1 Background

The mass production of synthetic polymers, commonly known as plastic, began in the early 1950s [1] and has steadily grown, reaching a global annual output of approximately 413.8 million tonnes by 2023 [2]. Because of its affordability, versatility, and unrivaled properties, plastic has cemented itself as an essential piece of the backbone of the modern economy [3]. While its attributes, such as corrosion resistance, chemical stability, electrical insulation, durability, and longevity, make plastic thrive across numerous industries, the same properties make it detrimental to the environment.

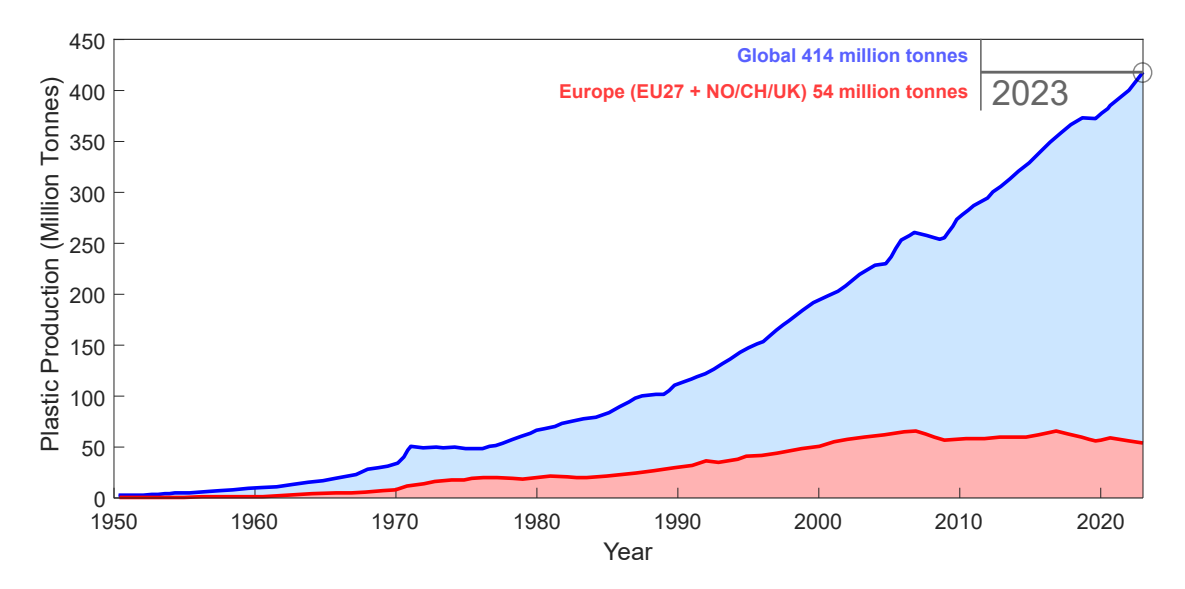


Figure 1.1: Illustration of the annual growth in plastic production since its inception in 1950 to 2023 [2], [4]. Two regions are compared, Europe (red) to the rest of the world (blue). The European data includes the 27 member states in the European Union, as well as Norway, Switzerland, and the United Kingdom. These results show that plastic production rates have been relatively constant in the EU for the last decade due to strict environmental regulations, higher recycling rates, implementation of circular economy strategies, and outsourcing plastic production. In contrast, plastic production continues to grow rapidly in the rest of the world.

Due to low recycling rates and inadequate waste management systems, much of this plastic has entered the marine environment [5]. Global estimates for the annual leakage of plastic waste into aquatic environments such as rivers and oceans have surpassed 23 million tonnes [6]. Previous studies indicate that

the majority of plastic present in the ocean exists in the form of microplastics. The term microplastics refers to plastic particles between 1 mm and 1 μm in size [7]. Such particles are either manufactured at such sizes for commercial use (primary microplastics) [8] or formed due to the breakdown of plastic products in a marine environment (secondary microplastics) [9]. The prospect of using numerical models to shed valuable insight into the transport and fate of microplastics has been an active research area in recent decades [10].

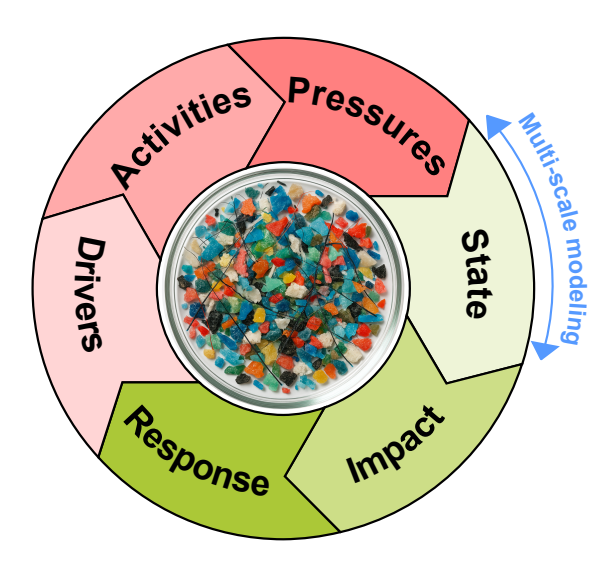


Figure 1.2: Depiction of the different components of the DAPSIR framework, highlighting the connection between elements and the role of multi-scale modeling to capture the *State* of a marine environment. The picture of microplastics in a petri dish is generated using AI tools.

1.2 DAPSIR

The classical DAPSIR (*Drivers*, *Activity*, *Pressures*, *State*, *Impact*, *Response*) framework is used here to contextualize the contributions, particularly in modeling the environmental *State*, within a broader framework for understanding microplastic pollution in marine environments [11]. As a surface-level conceptual framework, it can organize knowledge across disciplines for environmental assessment [12]. The OSPAR Quality Status Report 2023 [13] is a practical application of the DAPSIR framework, demonstrating its ability to structure comprehensive environmental assessments. Fig. 1.2 illustrates the graphical

relationship between the different components of the DAPSIR framework and the role of multi-scale modeling in capturing the *State* of a marine environment. Additional details on each element within the DAPSIR framework in the context of microplastic pollution are provided below.

- **Drivers:** The social and economic factors governing plastics' production and use. The most common drivers include consumer lifestyle, urbanization, industrialization, global trade, and population growth.
- Activities: Human activities that contribute to microplastic release into aquatic systems. Human activities involving microplastics can be linked to different industries such as packaging, construction, healthcare, transportation (automotive and shipping), fishing, agriculture, etc. [14]
- Pressures: Microplastic emissions into the marine environment directly resulting from human activities. Examples include tire and brake wear from the automotive sector, building paint from construction activities, synthetic fibers discharged during laundry activities, mishandling of plastic pellets, and plastic residue from fishing gear and marine coatings used in the shipping industry [15]. While microplastics from the shipping sector enter the aquatic environment directly, the remaining sources enter through sewage overflows, freshwater sediments, soil, and inadequate waste management systems.
- State: The environmental status refers to the physical and biological condition of a marine environment that influences the transport and fate of microplastics. From a policy and ecological monitoring context, environmental status is assessed under frameworks such as the Marine Strategy Framework Directive (MSFD) [16], specifically Descriptor 10 [17], which addresses marine litter, including microplastics. Multi-scale modeling plays a central role in resolving the environmental status by capturing processes such as advection, diffusion, biofouling, and stratification, and quantifying their impact on the fate of microplastics. These simulations complement ecological monitoring efforts, offering insights into microplastics' spatial and temporal distributions that are otherwise difficult to observe through field measurements.
- **Impacts:** Accounts for the effects of an altered environmental state on aquatic ecosystems and adverse impacts on human health. The ingestion

of microplastics can harm the health of marine biota, such as zooplankton, fish larvae, and sea urchins, causing abnormalities in their growth, development, and reproduction [18]. Microplastics also adversely impact phytoplanktons, the ocean's primary producers, reducing their photosynthesis rates and growth [19]. More concerning is the potential for microplastics to act as vectors for numerous pollutants, such as heavy metals [20] and persistent organic compounds [21]. This creates a pathway for harmful contaminants to enter the human body through seafood consumption [22].

• Responses: Actions aimed at mitigating pressures or reducing the impacts of microplastics. This can be achieved through policies and regulations, technological innovations, changing lifestyles, environmental monitoring, and improved waste management procedures and recycling rates. A recent example of regulatory progress is the EU Council's adoption of a general guideline for a regulation to prevent plastic pellet spillage across the supply chain, aiming to reduce microplastic pollution by up to 74 % [23].

1.3 A multi-scale modeling framework

Understanding the fate of microplastics in the ocean requires capturing numerous physical and biological processes that operate across vastly different spatial and temporal scales [24]. Due to its complexity, it represents one of the most interesting and challenging problems in environmental fluid mechanics. From microscale particle-fluid interactions governed by turbulence to mesoscale dynamics driven by oceanic physical and biological processes to large-scale motion influenced by ocean currents, no single modeling approach can capture all relevant scales simultaneously due to computational limitations. A flow-resolving method, such as Direct Numerical Simulations (DNS), is necessary to study flow behavior [25] and particle-fluid interactions [26] at the smallest scales. DNS has the capability to resolve all relevant flow structures and has therefore been widely used to investigate the fundamental mechanisms governing oceanic flows [27]. Large-scale numerical simulations for tracking microplastics are on the opposite end of the modeling spectrum. These models typically use Lagrangian particle tracking (LPT) models to track microplastic particles coupled with Ocean General Circulation Models (OGCM) that provide environmental forcing such as wind stresses, temperature fields, sea-floor depths, and surface currents [28], [29]. They serve as a powerful tool to explain the driving mechanisms behind observations in the real world; guide future field campaigns by identifying potential regions of particle accumulation, serve as a visual aid for communicating scientific findings to broader audiences, and support mitigation strategies by exploring "what if" scenarios.

In 2019, a workshop at the Les Houches School of Physics in France brought together leading experts in environmental fluid mechanics to develop a road map identifying key knowledge gaps that must be addressed to support progress toward the Sustainable Development Goals outlined in the 2030 Agenda for Sustainable Development by the United Nations. As an outcome of this workshop, a paper titled "Confronting the Grand Challenges of Environmental Fluid Mechanics " was later published [30]. In this paper, the authors highlight considerable advances in our understanding of the fundamental mechanisms driving ocean turbulence, both through DNS and field observations. However, they show a growing disconnect between these advances and their subsequent implementation into predictive tools for addressing the UN Sustainable Development Goals. In the context of microplastic pollution, a closer look at existing large-scale models reveals that this limitation exists with many phenomena and processes that influence particle transport. Hence, this thesis aims to address this knowledge gap by developing a multi-scale modeling framework (Fig. 1.3) that bridges high-resolution flow simulations with large-scale modeling tools for predicting the fate of microplastics in marine ecosystems.

The use of DNS to explore microscale dynamics and large-scale particle tracking models to study the fate and transport of microplastics in realistic ocean conditions is well-established. However, a significant knowledge gap exists in understanding how to effectively translate insights from high-resolution DNS studies to large-scale simulations [30]. The identified gap is addressed by introducing an intermediate or transitional modeling scale that doesn't resolve all the turbulence in the flow, nor incorporates all the complex environmental forcing from an OGCM-coupled LPT model. The intermediate modeling scale has two main objectives. Firstly, this modeling approach is a platform to evaluate detailed correlations derived from DNS studies before implementation in large-scale models. Secondly, large-scale simulations are

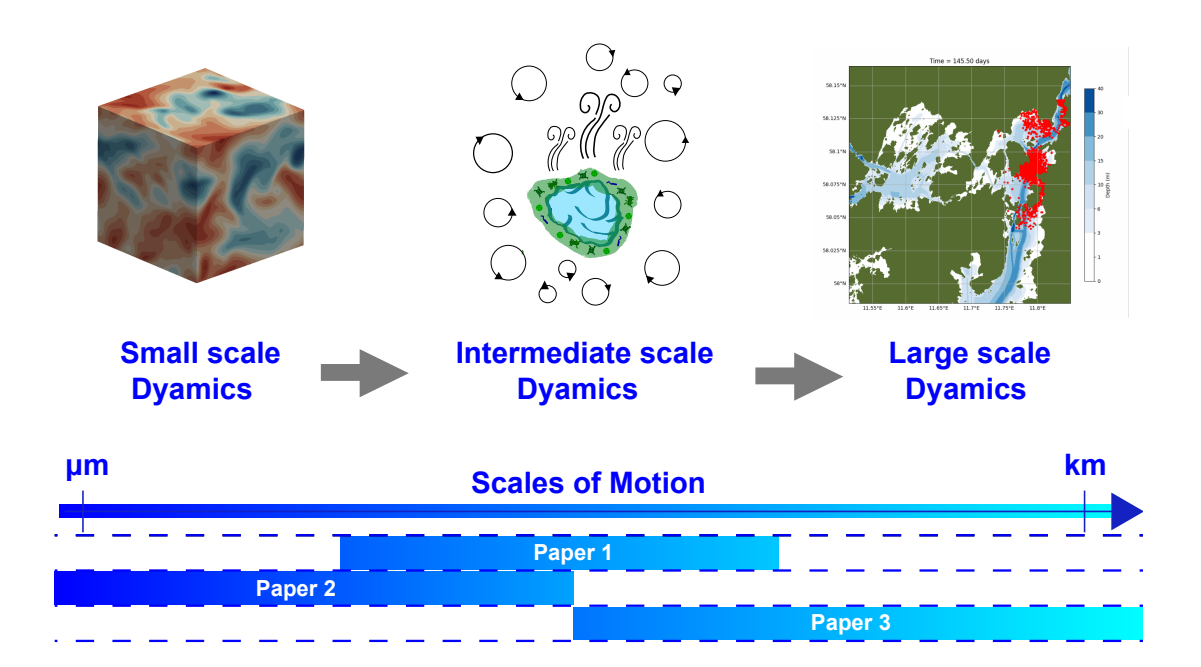


Figure 1.3: A visualization of the proposed multi-scale modeling framework, with each component linked to a corresponding paper in the thesis. On the left, a snapshot from a pseudo-spectral DNS illustrates stratified turbulence (**Paper 2**). The center image shows a biofouling microplastic particle settling in a turbulent flow environment (**Paper 1**). On the right, a simulation snapshot captures microplastic transport in the Orust-Tjörn fjord system (**Paper 3**).

too dynamic to understand how individual processes affect particle motion. Therefore, intermediate-scale simulations can use controlled numerical setups to isolate and investigate specific variables or processes in a marine environment that influence the fate of microplastics. Such an approach enables a more transparent and focused analysis of how they affect particle dynamics. By reducing the environmental complexity of real-world conditions, the proposed intermediate-scale models can systematically explore individual factors influencing microplastic motion, laying the groundwork for more robust parameterizations in large-scale transport models.

1.4 Thesis outline

The thesis is structured in two main parts: an overview providing an extended summary of the research, followed by a collection of scientific papers

produced during the research study. The overview comprises five thematic sections, each addressing a key aspect of the research study. Chapter 1 provides a background to the research study, placing it in the broader context of microplastic pollution and highlighting the motivation and necessity for this study. Chapter 2 explores how direct numerical simulations can resolve and analyze small-scale dynamics in oceanic conditions. Chapter 3 will discuss the role of the intermediate modeling scale in bridging the gap between small-scale dynamics and large-scale simulations. Chapter 4 will introduce the development of a new large-scale microplastic tracking software named "MPDrift." The final section, Chapter 5, reflects on the proposed multi-scale modeling framework and discusses its importance in environmental impact assessment.

1.5 Aim and objectives

The aim of this thesis work is to develop a multi-scale modeling framework for numerically investigating the fate of microplastics in marine environments. To accomplish this goal, investigations are carried out at three different scales, where the following objectives are pursued.

- 1. Investigate the potential of using flow resolving simulations to capture detailed physics of stratified ocean turbulence and particles settling in such complex marine environments.
- 2. To demonstrate the role of an intermediate modeling scale, study interactions between turbulence and biofouling with a focus on how they influence the settling dynamics of microplastics. Investigate the importance of using a detailed turbulence model to capture the impact of turbulence on biofouling rate.
- 3. Develop a large-scale microplastic tracking model and conduct a numerical case study of microplastic pollution in the fjord system surrounding Stenungsund. Use numerical predictions to explain field observations.

CHAPTER 2

Fully resolved flows

Direct numerical simulations are increasingly used in oceanographic applications to provide detailed descriptions of flow behavior and particle-fluid interactions that are difficult to capture using field measurements. Here, DNS methods are used to investigate how intermittent events in density-stratified flows can affect the range of forces experienced by a sinking microplastic particle. Motivated by the presence of instantaneous, adverse density gradients in stably stratified environments, a new set of governing equations is derived and numerically solved for particles settling in temperature-stratified flows where temperature increases with depth. These results reveal that particles experience a drag reduction under this condition, which, under certain assumptions, can be considered symmetric to drag enhancements observed in stable stratification. However, comparisons of the settling velocity of particles in stable and unstable stratified fluids show an asymmetric behavior. This difference becomes more prominent as the stratification strength increases, where the drag reduction under unstable conditions is higher than the drag enhancement for stable stratification.

2.1 Stratification

The ocean is a highly complex and dynamic environment where characteristic flow variables such as temperature and salinity can vary spatially and temporally [31]. Variations in these fields can result in a vertical density gradient, a phenomenon known as stratification [32]. Stratification inhibits vertical mixing, acting as a barrier and influencing the vertical distribution and exchange of nutrients, carbon, oxygen, and other gases across the water column [33]. Stratification also affects and controls primary productivity and biodiversity in aquatic ecosystems [34]. Understanding the fundamentals of stratification has been a highly pursued research area because of the highly complex nature of stratified flows and their importance to Earth's climate [35]. Particles settling in stratified flows also represent a typical process in marine environments [36]. Common examples include the settling of plankton, marine snow, and microplastics in the ocean [37]. Furthermore, field studies have reported higher concentrations of marine snow and microplastics within the pycnocline [24], [38], [39], a layer characterized by a strong vertical density gradient that can significantly influence particle transport and retention. Stratification has two notable impacts on settling particles [40]. Firstly, settling particles experience an enhanced drag in stratified fluids with a continuous density gradient [41]. Secondly, the wake behind the particle can change depending on particle characteristics and stratification strength. For spherical particles, seven distinct wake structures have been previously identified that closely relate to the Reynolds and Froude numbers of the flow [27]. Consequently, understanding the fundamentals of particle settling dynamics in stratified regions of the ocean is of significant importance, as this process must be accurately captured in large-scale models that track the transport of microplastics.

2.2 Pseudo-spectral DNS

Among the different types of numerical schemes to fully resolve turbulent flows, spectral methods stand out for geophysical flows as they offer high accuracy, efficiency, and the ability to handle periodic boundary conditions naturally [42]. This approach solves the governing Navier-Stokes equations in the Fourier space. Spatial derivatives are computed in the Fourier domain using fast Fourier transforms (FFTs). At the same time, the nonlinear term is

evaluated in the physical space and transformed back to the spectral domain, hence the name "pseudo-spectral." An in-house pseudo-spectral code is used here to perform forced homogeneous stratified flow simulations.

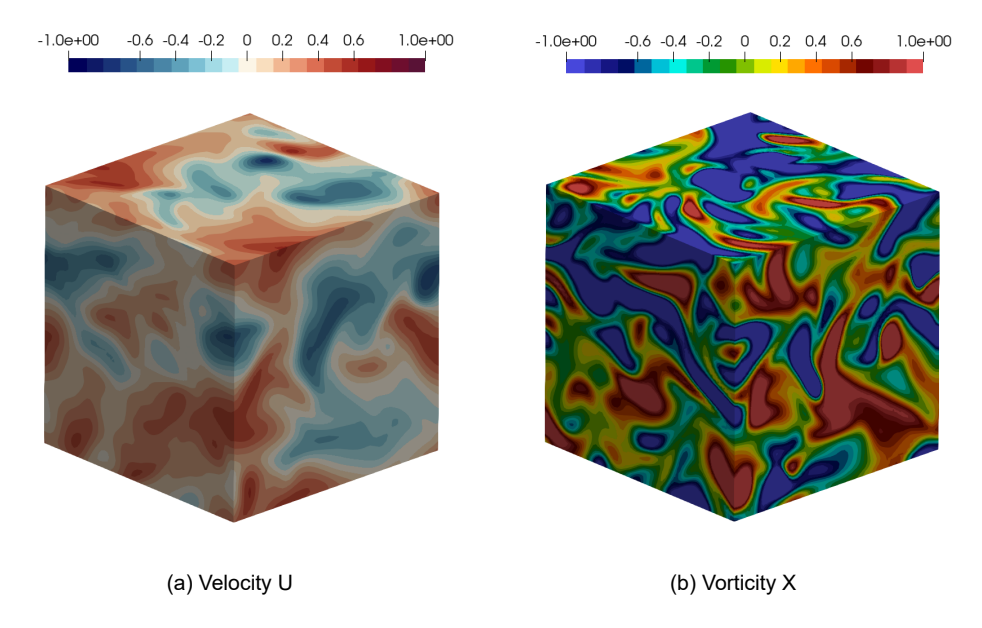


Figure 2.1: A snapshot of the U-velocity and X-vorticity fields generated during the pseudo-spectral analysis.

Assuming the fluid to be incompressible and Newtonian, the governing equations for a stratified fluid with the Boussinesq assumption for density can be stated as [43]:

$$\nabla \cdot \mathbf{u} = 0 \tag{2.1}$$

$$\frac{\partial \mathbf{u}}{\partial t} + \mathbf{u} \cdot \nabla \mathbf{u} = -\frac{\nabla p}{\rho_f} + v \nabla^2 \mathbf{u} - \frac{(\rho_f - \rho_0)}{\rho_0} g \, \mathbf{e}_z + \mathbf{f}_1$$
 (2.2)

while the density field is governed by:

$$\frac{\partial \rho_f}{\partial t} + \mathbf{u} \cdot \nabla \rho_f = \nabla \cdot (\kappa \nabla \rho_f) - \frac{\partial \bar{\rho_f}}{\partial z} u_z$$
 (2.3)

where **u** is the velocity, p is the pressure, ρ_f is the fluid density, ρ_0 is a constant reference fluid density, v is the kinematic viscosity, κ is the diffusivity, g is the gravitational acceleration, $\gamma_{\rho} = \partial \bar{\rho_f}/\partial z$ is the vertical mean

density gradient, u_z is the vertical velocity component, \mathbf{f}_1 is the external force that is required to maintain a statistically stationary state of stratified turbulence, and \mathbf{e}_z is a unit vector in the vertical direction. The flow is assumed to be stably stratified, so the density increases with depth. A typical flow visualization of the resolved stratified turbulence is shown in Fig. 2.1. In the present model, the aliasing error is reduced using the classical 2/3 rule for dealiasing when evaluating the nonlinear term in the physical space. The simulations are performed on a computational grid with a resolution of 256³. A low-storage Runge-Kutta scheme is used for temporal discretization, and the Adam-Bashforth approximation is used to solve the nonlinear term. Stochastic forcing is isotropically applied on the first shell of wave numbers ($|\mathbf{k}| = 1$). The stratification effects in the fluid are assumed to be driven by variations in temperature, which is reflected in the numerical setup by specifying a Prandtl number (Pr) of 7. Six oceanographic regions are reconstructed for comparative analysis, each characterized by a representative vertical density gradient (γ_o) and turbulent dissipation rate (ϵ) , as summarized in Tab. 2.1. It should be noted that due to the highly transient nature of turbulence, similar values may also occur in other regions.

Region	$\gamma_{\rho}~(\mathrm{kg/m^4})$	$\epsilon (\mathrm{W/kg})$	$\eta \text{ (mm)}$	Re_T
Mixed layer (ML)	-0.001	$1\cdot 10^{-6}$	1.11	100
Thermocline/Pycnocline (TP)	-0.01	$1 \cdot 10^{-8}$	3.63	107
Deep ocean (DO)	-0.0001	$1 \cdot 10^{-10}$	11.4	111
Near seafloor (NS)	-0.001	$1 \cdot 10^{-6}$	1.11	100
Fjords and estuaries (FE)	-0.1	$1 \cdot 10^{-6}$	1.11	109

Table 2.1: Overview of simulation parameters for each test case. Data for five oceanographic regions are included: mixed layer [44], thermo/pycnocline [45], [46], Deep ocean [47]–[49], near seafloor [50], and fjords and estuaries [51]–[53]. η represents the Kolmogorov length scale and Re_T is the Taylor Reynolds number.

Here, the mixed layer, pycnocline, and deep ocean are a three-layer vertical structure representative of the ocean's water column [54]. The mixed layer is on the surface and is governed by wind-driven turbulence. The thermocline/pycnocline layer is below the mixed layer and has strong density gradients. The deep ocean, situated below the pycnocline, is insulated from the atmosphere. Hence, it consists of weak stratification and turbulence effects. It

is assumed that the kinematic viscosity is $1.2 \times 10^{-6} \, m^2/s$, which corresponds to a sea water temperature of $10\,^{\circ}\mathrm{C}$ [55], [56]. The density of seawater is assumed to be 1000 kg/m^3 for simplicity, and gravitational acceleration was set to 9.81 m/s^2 .

2.3 Intermittency of density gradient

The pseudo-spectral DNS code serves one purpose: evaluating the range of density gradients in the five aforementioned oceanic regions. This is achieved through a simple yet powerful approach: plotting probability density functions (PDFs). PDFs give valuable insight into the statistics of how flow variables fluctuate under different turbulent conditions. Fig. 2.2 illustrates the PDFs of the normalized vertical density gradients $(\gamma_{\rho}/\bar{\gamma_{\rho}})$.

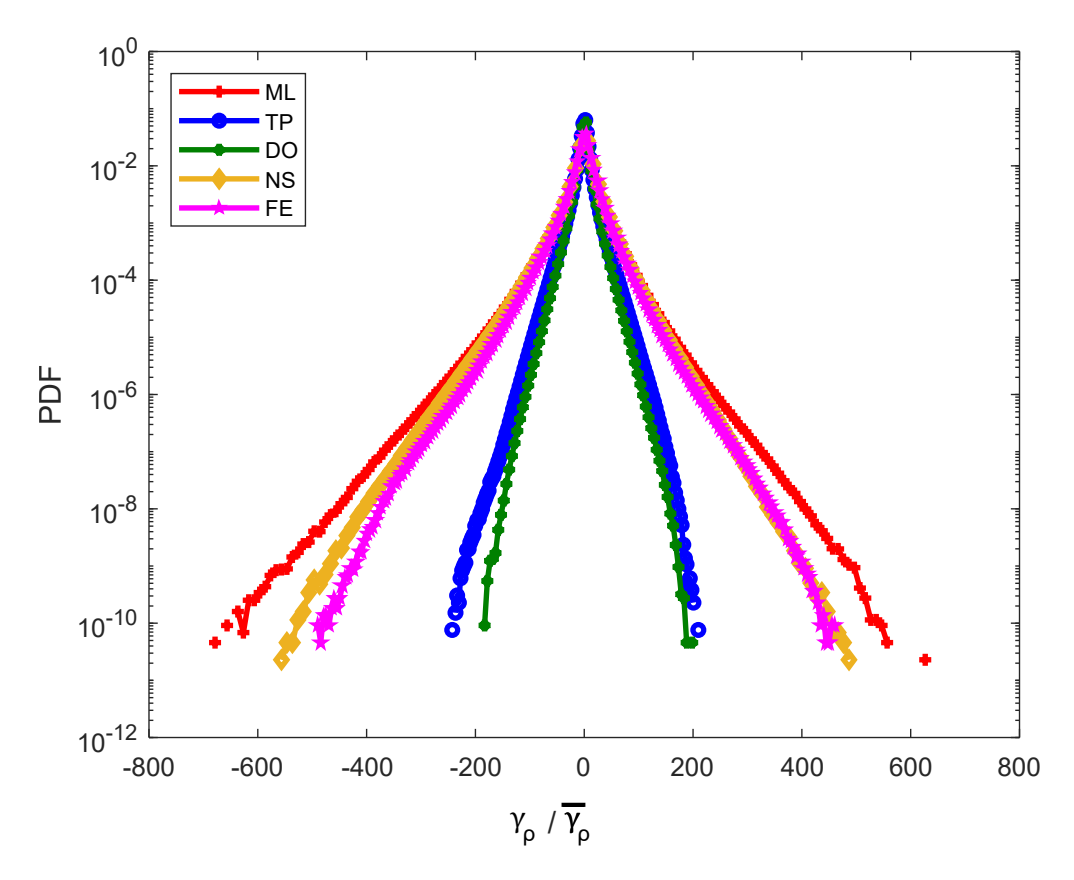


Figure 2.2: Illustration of the PDFs of the fluctuating density gradients normalized against the mean value for the five explored oceanographic regions.

These results show that γ_{ρ} is highly non-Gaussian. For the case of ML, NS, and FE, where ϵ is set to $10^{-6} W/kg$, the fluctuating density gradients are shown to go as high as 400-600 times the mean density gradient. However, among these three scenarios, the peak value is highest for $ML(\gamma_{\rho})$ $-0.001 \, kg/m^4$) and lowest for $FE(\gamma_{\rho} = -0.1 \, kg/m^4)$. Among these three cases, the background γ_{ρ} is lowest for the case of NS. This represents essentially homogeneous turbulence with a weak stratification effect. As γ_{ρ} increases (as in the case of ML), the density field becomes more structured, but turbulence remains strong enough that the peak density fluctuations continue to increase relatively. However, as γ_{ρ} increases even further to $-0.1 \, kg/m^4$, the flow becomes layered, and the stratification effect dominates and suppresses vertical motion. Turbulence effects are now reduced, and the flow can no longer produce the same relative fluctuations in the density gradient as observed with the ML case. As a result, the peak values for FE are lower than those of ML and NS. Fig. 2.2 also confirms that ϵ has a much higher impact than γ_{ρ} on peak density perturbations.

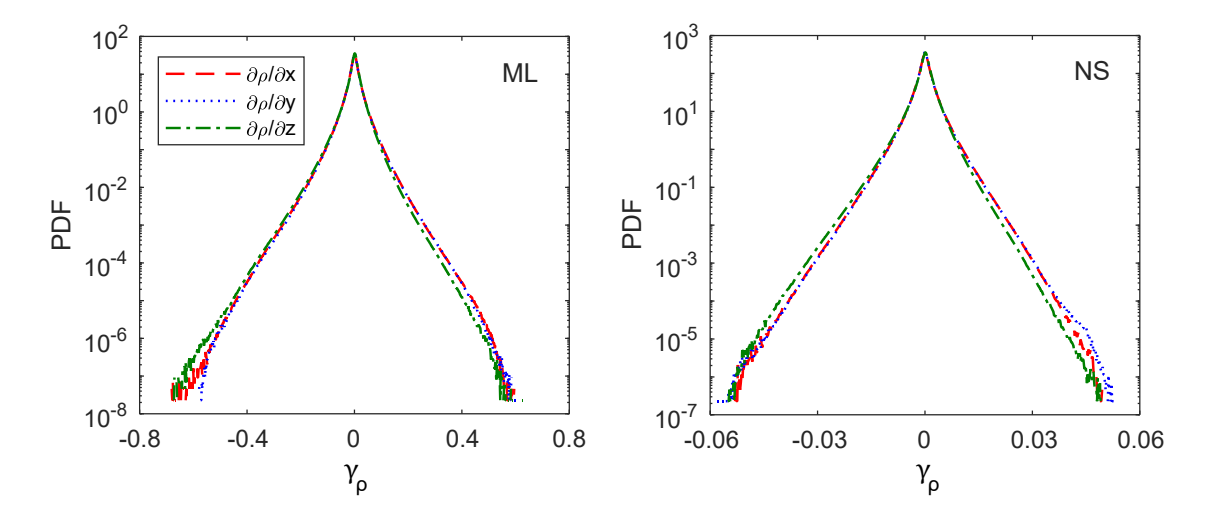


Figure 2.3: Comparisons between the PDFs of the density gradients in the three spatial directions for the case of ML and NS.

Fig. 2.3 visualizes the density gradients across the three spatial directions to evaluate skewness and symmetry for ML and NS. These results show that the density gradients in the lateral directions ($\partial_x \rho$ and $\partial_y \rho$) are symmetric. The characteristic flow feature in this case is that the vertical density gradient is negatively skewed. To quantify the skewness, we use the following expression.

$$S = \frac{E[(X - \mu)^3]}{\sigma^3}$$
 (2.4)

where X is the fluctuating density gradients, μ is the mean density gradient, and σ is the standard deviation. The skewness of the density gradients in the x, y, and z directions is presented in Tab. 2.2.

	ML	NS
$\partial_x \rho$	0.0034	0.0034
$\partial_y ho$	0.0034	0.0034
$\partial_z ho$	-0.6517	-0.1729

Table 2.2: Summary of skewness observed with the density gradients in x, y, and z directions.

It is evident that the density gradients in the lateral directions are almost symmetrical, signified by the very low skewness values, and the vertical density gradient is highly skewed, with similar magnitudes to the results of Kop [57]. Similar observations were made with the remaining oceanographic cases.

2.4 DNS with Immersed Boundary Method

The asymmetric and non-Gaussian nature of vertical density gradients presents an interesting case for investigating how density perturbations affect the forces acting on particles settling in stratified fluids. However, the results demonstrated that stably stratified fluids can give rise to $\gamma_{\rho} < 0$ and $\gamma_{\rho} > 0$ instances, depending on local fluctuations in the density field. While particles settling in stratified flows with $\gamma_{\rho} < 0$ have been extensively studied, little is known about the opposite density gradient ($\gamma_{\rho} > 0$). A numerical methodology is introduced to estimate the forces acting on a particle settling in a stratified fluid with high accuracy. The DNS approach used for this purpose is the Immersed Boundary Method (IBM) [58]–[60]. Fig. 2.4a illustrates a representative figure of the numerical setup.

The density perturbations are assumed to be driven by variations in the temperature field, resulting in a constant temperature gradient in the vertical direction. Similar to the previous study, a Pr value of 7 is utilized, which

corresponds well with stratified flows driven by temperature gradients. In the case of stable stratification ($\gamma_t = \partial T/\partial z$), where the colder and heavier fluid is at the bottom, the non-dimensional governing equations are written as [61]:

$$\nabla \cdot \mathbf{u} = 0 \tag{2.5}$$

$$\frac{\partial \mathbf{u}}{\partial t} + \mathbf{u} \cdot \nabla \mathbf{u} = -\nabla p + \frac{1}{Re_p} \nabla^2 \mathbf{u} + \frac{Ra}{Re_p Pe} T \mathbf{e}_z + \mathbf{f}_2$$
 (2.6)

$$\frac{\partial T}{\partial t} + \mathbf{u} \cdot \nabla T + u_z - 1 = \frac{1}{Pe} \nabla^2 T \tag{2.7}$$

where \mathbf{u} , p and T are dimensionless velocity, pressure, and temperature, respectively. This system of equations is defined using three dimensionless numbers: particle Reynolds number, $Re = U_p d/\nu$, Péclet number, $Pe = U_p d/\kappa_t$, and $Ra = g\beta\gamma_t d^4/\kappa_t\nu$, where β is the thermal expansion coefficient, κ_t is the thermal diffusivity, U_p is the particle settling velocity, d is the particle diameter, and f_2 is the IBM force that is used to indirectly apply the no-slip and no-penetration boundary conditions near the particle. The velocity of the spherical particle has a translational and rotational component $(U_p = u_p + \omega_p \times r)$.

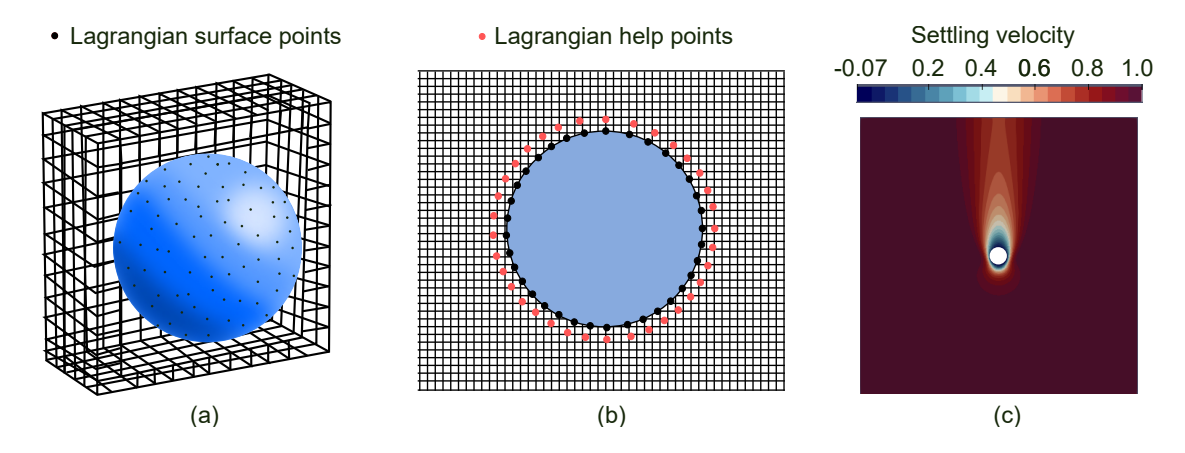


Figure 2.4: An illustration of the (a) immersed boundary method for a particle with Lagrangian points inside an Eulerian grid (adapted from [58]), (b) Lagrangian help points used to implement temperature gradient boundary condition on the particle surface (adapted from [62]), and (c) typical W velocity field around a sinking particle.

After accounting for the mass of fictitious fluid in the particle and using IBM, the governing equations for the particle motion can be written as [58]:

$$\rho_p U_p \frac{du_p}{dt} \approx -\rho_0 \sum_{l=1}^{N_L} \mathbf{F}_l \Delta U_l + \rho_0 \frac{d}{dt} \left(\int_{U_p} \mathbf{u} dV \right) + (\rho_p - \rho_f) U_p \mathbf{g}$$
 (2.8)

$$I_{p}\frac{d\omega_{p}}{dt} \approx -\rho_{0} \sum_{l=1}^{N_{L}} r_{l} \times \mathbf{F}_{l} \Delta V_{l} + \rho_{0} \frac{d}{dt} \left(r \times \int_{U_{p}} \mathbf{u} dV \right)$$
 (2.9)

The first two terms on the right-hand side account for the IBM force and torque acting on the particle. The third term in (2.8) denotes the buoyancy force exerted on the particle due to the inertia effects of the fluid trapped within the particle. The following boundary conditions are valid for the dimensionless fields, assuming the particle is fixed in space [61].

$$\mathbf{u}\left(|x| = \frac{1}{2}\right) = 0, \ \partial_r T\left(|x| = \frac{1}{2}\right) = -2z, \ \mathbf{u}_{\infty} = e_z, \mathbf{T}_{\infty} = 0.$$
 (2.10)

The above boundary conditions show that a temperature gradient of -2z must be enforced on the particle's surface. This is achieved using Lagrangian help points positioned at a distance of Δx outwards from the Lagrangian points on the particle, as shown in Fig. 2.4b, similar to the approach by Lupo et al. [62]. The temperature at these help points (T_L^H) is estimated by interpolation from neighboring grid points. With the first-order approximation between these help points and the Lagrangian help points on the particle's surface, the temperature at the particle's surface (T_L^S) can be estimated as:

$$T_L^S = T_L^H - 2z\,\Delta x\tag{2.11}$$

2.5 Particles settling in unstable stratified flows (Derivation)

A new set of governing equations is derived here for particles settling in stratified fluids where warmer and lighter fluid is at the bottom ($\gamma_t < 0$) is derived. Considering a frame of reference moving with the particle, the far-field velocity and temperature would obey:

$$\mathbf{u}_{\infty}^* = U_{\infty} \, e_z \tag{2.12}$$

$$T_{\infty}^{*} = T_{0}^{*} - \gamma_{t}z + \gamma_{t}U_{\infty}t + T^{*'}$$
(2.13)

where T_0^* refers to a reference temperature, $T^{*'}$ describes temperature perturbations from far-field, and γ_t is the absolute value of the temperature gradient $(|\gamma_t|)$. The superscripts * denote that the variables are dimensional. Along with these far-field conditions, the governing equations for incompressible Navier-Stokes flow with Boussinesq assumptions can be written as follows.

$$\nabla \cdot \mathbf{u}^* = 0 \tag{2.14}$$

$$\frac{\partial \mathbf{u}^*}{\partial t^*} + \mathbf{u}^* \cdot \nabla \mathbf{u}^* = -\frac{\nabla p^*}{\rho_f} + \upsilon \nabla^2 \mathbf{u}^* + g \beta T^{*'} \mathbf{e}_z$$
 (2.15)

$$\frac{\partial T^{*'}}{\partial t^*} + \mathbf{u}^* \cdot \nabla T^{*'} - \gamma_t (u_z^* - U_\infty) = \kappa_t \nabla^2 T^{*'}$$
 (2.16)

The boundary conditions also include a no-slip/no-flux boundary condition on the sphere's surface and the far field temperature fluctuations are assumed to be zero. The particle is considered to be thermally insulated, with no heat flux across its surface. However, an additional boundary condition is required for the temperature at the particle's surface relative to the surrounding fluid for numerical stability. We derive this boundary condition by applying the radial derivative of Eq. 2.13 to the particle's surface.

$$\frac{\partial(T_{\infty}^{*})}{\partial r} = \frac{\partial(T_{0}^{*})}{\partial r} - \frac{\partial(\gamma_{t}z)}{\partial r} + \frac{\partial(\gamma_{t}U_{\infty}t)}{\partial r} + \frac{\partial(T^{*'})}{\partial r}$$
(2.17)

At the surface of the particle, the first, second, and fourth terms become zero, leaving us with:

$$\frac{\partial (T^{*'})}{\partial r} = \gamma_t \frac{\partial z}{\partial r}.$$
 (2.18)

Using mathematical manipulation, we can rewrite $\frac{\partial z}{\partial r}$ as follows:

$$\frac{\partial z}{\partial r} = \frac{z}{|r|} = \frac{2z}{d}. (2.19)$$

Substituting Eq. 2.19 in Eq. 2.18 tells us that the radial temperature gradient at the particle's surface is equal to $2\gamma_t z/d$. All the boundary conditions accompanying the governing set of equations when setting up the numerical model can be summarized as follows.

$$\mathbf{u}^* \left(|\mathbf{x}^*| = \frac{d}{2} \right) = 0, \ \partial_r T^{*'} \left(|\mathbf{x}^*| = \frac{d}{2} \right) = \frac{2\gamma_t z}{d}, \ \mathbf{u}_{\infty}^* = e_z, \ T_{\infty}^{*'} = 0.$$
 (2.20)

The following characteristic scaling relations are used to rewrite the governing system of equations in dimensionless form.

$$\mathbf{u} = \frac{\mathbf{u}^*}{U_{\infty}}, \ p = \frac{p^*}{\rho U_{\infty}^2}, \ T = \frac{T^{*'}}{\gamma_t d}, \ \mathbf{x} = \frac{\mathbf{x}^*}{d}, t = \frac{U_{\infty} t^*}{d}$$
 (2.21)

Applying these relations to the continuity equation is straightforward, yielding the dimensionless form:

$$\nabla \cdot \mathbf{u} = 0. \tag{2.22}$$

Afterward, the Navier-Stokes momentum equation is transformed using the above scaling relations, where substituting Eq. 2.21 into Eq. 2.15 yields:

$$\frac{U_{\infty}^{2}}{d}\frac{\partial \mathbf{u}}{\partial t} + \frac{U_{\infty}^{2}}{d}\mathbf{u} \cdot \nabla \mathbf{u} = -\frac{\rho f U_{\infty}^{2}}{\rho f d} \nabla p + \frac{v U_{\infty}}{d^{2}} \nabla^{2}\mathbf{u} + g \beta \gamma_{t} dT \mathbf{e}_{z}$$
(2.23)

Multiplying Eq. 2.23 with d/U_{∞}^2 simplifies it to:

$$\frac{\partial \mathbf{u}}{\partial t} + \mathbf{u} \cdot \nabla \mathbf{u} = -\nabla p + \frac{v}{U_{\infty} d} \nabla^2 \mathbf{u} + \frac{g \beta \gamma_t d^2 T}{U_{\infty}^2} \mathbf{e}_z$$
 (2.24)

The above equation is characterized by three dimensionless numbers: the Reynolds number, the Péclet number, and the Rayleigh number. The coefficients of the viscous term can be replaced by 1/Re. The coefficient of the buoyancy term is expressed as the following combination:

$$\frac{g \,\beta \,\gamma_t \,d^2 \,T}{U_{\infty}^2} = \frac{g \,\beta \,\gamma_t \,d^4}{\kappa_t \nu} \times \frac{\nu}{U_{\infty} d} \times \frac{\kappa_t}{U_{\infty} d} \tag{2.25}$$

where the first, second, and third terms of the right-hand side can be replaced by Ra, 1/Re, and 1/Pe, respectively. Substituting these dimensionless numbers and accounting for the IBM force gives us the following dimensionless Navier-Stokes momentum equation.

$$\frac{\partial \mathbf{u}}{\partial t} + \mathbf{u} \cdot \nabla \mathbf{u} = -\nabla p + \frac{1}{Re} \nabla^2 \mathbf{u} + \frac{Ra}{Re Pe} \mathbf{e}_z + \mathbf{f}_2$$
 (2.26)

As for the temperature field, substituting Eq. 2.21 into Eq. 2.16 gives:

$$\frac{\gamma_t \not d U_{\infty}}{\not d} \frac{\partial T}{\partial t} + \frac{U_{\infty} \gamma_t \not d}{\not d} \mathbf{u} \cdot \nabla T - \gamma_t U_{\infty}(u_z - 1) = \frac{\kappa_t \gamma_t \not d}{\partial f} \nabla^2 T.$$
(2.27)

Dividing all the terms with $\gamma_t U_{\infty}$ gives the following expression:

$$\frac{\partial T}{\partial t} + \mathbf{u} \cdot \nabla T - (u_z - 1) = \frac{\kappa_t}{U_\infty d} \nabla^2 T.$$
 (2.28)

The coefficient of the diffusion term in the temperature transport equation is equal to 1/Pe. This substitution completes the dimensionless temperature transport equation.

$$\frac{\partial T}{\partial t} + \mathbf{u} \cdot \nabla T - (u_z - 1) = \frac{1}{Pe} \nabla^2 T \tag{2.29}$$

The corresponding boundary conditions for this system of equations are similar to Eq. 2.20. The boundary condition for radial temperature gradient at the particle's surface has to be modified to account for dimensionless

temperature. Therefore, the scaling relation for temperature from Eq. 2.21 is introduced to the radial temperature gradient boundary condition in Eq. 2.20 which gives:

$$\mathcal{A}d\frac{\partial T}{\partial r} = \frac{2\mathcal{A}z}{d}.$$
 (2.30)

Eq. 2.30 can be rearranged to give:

$$\frac{\partial T}{\partial r} = \frac{2z}{d^2}. (2.31)$$

Eq. 2.31 can be further simplified by defining the numerical model using a unit particle diameter. The final boundary conditions required to satisfy the dimensionless governing equations are shown below.

$$\mathbf{u}\left(|\mathbf{x}| = \frac{1}{2}\right) = 0, \ \partial_r T\left(|\mathbf{x}| = \frac{1}{2}\right) = 2z, \ \mathbf{u}_{\infty} = e_z, T_{\infty} = 0$$
 (2.32)

Temperature perturbations in a stratified flow introduce two key modifications to the dimensionless governing equations for a settling particle. First, a source term, $(Ra/RePe) \mathbf{e}_z$, is added to the Navier-Stokes momentum equation to account for buoyancy variations. Notably, this term remains unaffected by adverse temperature gradients $(\gamma_t < 0)$. The second modification involves an additional source term, $u_z - 1$, in the governing equation for the temperature field. Our derivations show that this term becomes $-(u_z - 1)$ for particles settling in stratified flows with an adverse temperature gradient. Furthermore, for the governing equations that consider a frame of reference that moves with the particle, and the particle is fixed in space, an additional consideration must be made regarding the temperature gradient at the particle's surface with respect to the surrounding fluid. Lee et al. [61] demonstrated that this boundary condition reduces to $\partial_r T(|x| = 1/2) = -2z$ for stratified fluids with $\gamma_t > 0$. For the case of $\gamma_t < 0$, our derivations show that this boundary condition reduces to $\partial_r T(|x| = 1/2) = 2z$.

2.6 Drag enhancement and reduction

The drag experienced by a particle settling in stratified flows has historically been a widely explored research area [63]. Here, the governing equations derived in Sec. 2.5 are used to evaluate the drag acting on a particle settling in a flow with an inverse temperature gradient ($\gamma_t < 0$). First, the numerical results of Lee et al. [61] are used to validate the model for the case of stable stratification, and the comparisons are visualized in Fig. 2.5.

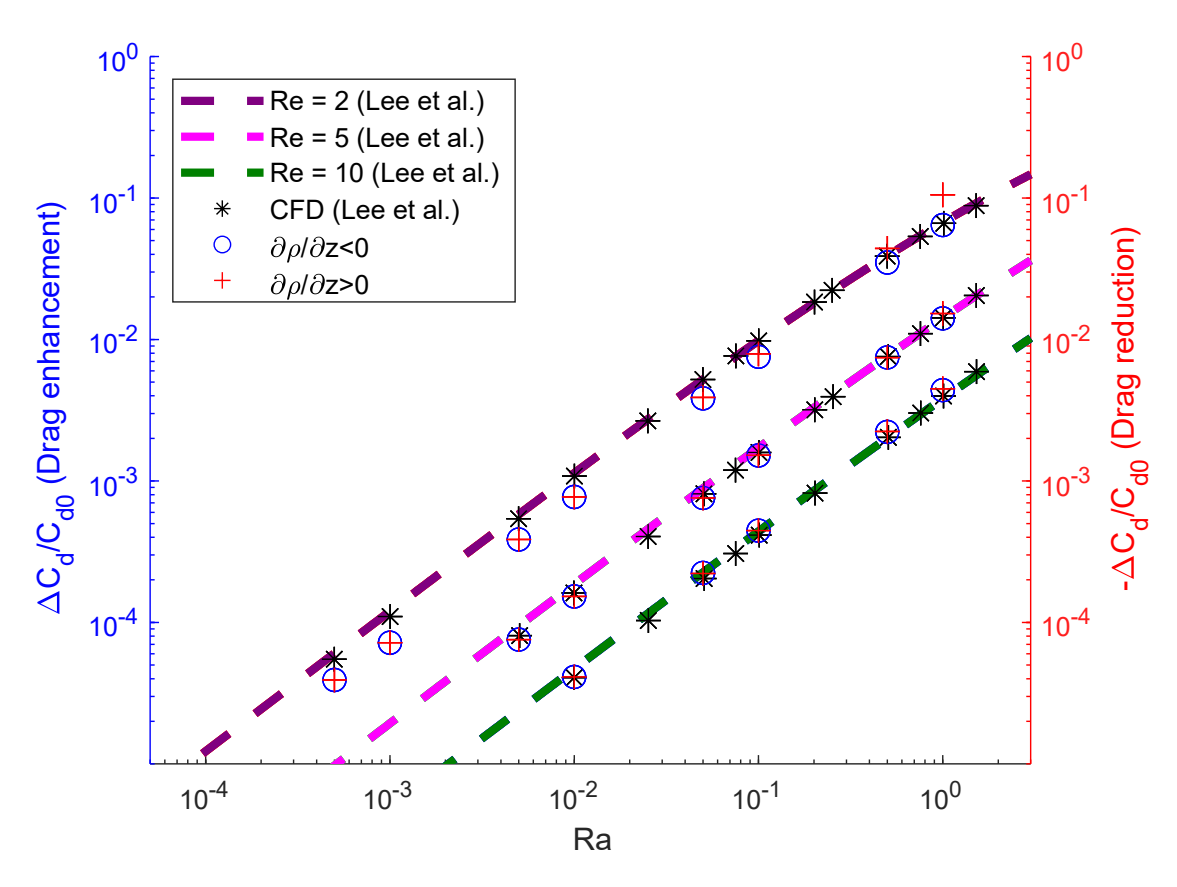


Figure 2.5: Drag modification for a particle in a stratified flow. For $\partial \rho/\partial z < 0$, the drag enhancement $(\Delta C_d/C_{d0})$ is shown, while for the $\partial \rho/\partial z > 0$ cases, the drag reduction $(-\Delta C_d/C_{d0})$ is plotted. The numerical results and empirical correlations of [61] at Pr = 7 for the $\partial \rho/\partial z < 0$ cases are included for comparison.

Lee et al. [61] proposed a new expression for drag enhancement using their numerical results for $0.01 < Re_p < 10$ and $10^{-4} < Ra < 1.5$:

$$a = 0.00752 - 0.02049 Re + 2.00936 Re_p^2$$

$$b = -0.21154 + 0.56102 Re + 0.49302 Re_p^2$$

$$c = 2.56921 + 4.6469 \left(1 - \exp^{-0.17907 Re_p}\right)$$

$$\frac{C_D}{C_{D,0}} = 1 + \frac{Ra}{a + bRa^{1/3} + cRa^{2/3}}$$
(2.33)

where C_d and $C_{d,0}$ are the drag acting on a particle in stratified and unstratified flow, respectively. As shown in Fig. 2.5, the results of Lee et al. [61] are in good agreement with the numerical predictions from the IBM model. Subsequently, the newly derived equations for the unstable stratification case are numerically evaluated. The results are plotted alongside the previous data in (Fig. 2.5), with a secondary y-axis introduced to quantify the change in drag. This axis is labeled "Drag reduction" as $\Delta C_D/C_{D,0}$ is negative in this case, indicating a reduction in drag. These results show that the change in drag between stable and unstable cases is symmetrical except for Ra = 0.5 and Ra = 1.0 at $Re_p = 2$. Further investigations revealed that the numerical stability of the unstable case is sensitive to the domain size, which can be attributed to the Rayleigh-Bénard instability that may arise in cases of unstable stratification. The expression for the Rayleigh number of the flow (Ra_D) in the absence of a particle can be stated as:

$$Ra_D = \frac{g\beta}{\nu\kappa_t} \Delta T L^3 \tag{2.34}$$

where L denotes the domain height, and ΔT is the temperature difference between the top and bottom surfaces of the domain. Eq. 2.34 shows that Ra_D scales with L^3 , and stability of Rayleigh-Bénard convection. However, since the governing equations are formulated with a stationary frame of reference to a settling particle, an explicit value for Ra_D cannot be directly obtained. Furthermore, as Re_p decreases, the particle's wake expands and extends to the lateral boundaries of the domain, which are subject to periodic boundary conditions. This interference can influence the numerically estimated drag force. Therefore, a larger domain is necessary to accurately resolve the flow physics around a settling particle as Re_p reduces. This presents a contradiction: while a flow with lower Re_p values requires a larger domain for sufficient resolution, preventing the Rayleigh–Bénard instability requires a smaller domain to maintain Ra_D at a subcritical value. Using the remaining results obtained from this numerical study, it is concluded that while it's not possible to accurately capture the drag force acting on particles as Re_p decreases, the results from $Re_p = 5$ and $Re_p = 10$ shows strong evidence that the drag acting on a particle is symmetric when comparing drag enhancement $(\gamma_t > 0)$ and reduction $(\gamma_t < 0)$. It is assumed that this relationship will also hold for low Reynolds numbers. The assumption is valid within the constraint of limited domain sizes and assumes that the near-wake dynamics are the main driving factors influencing particle sinking dynamics in the ocean. Furthermore, the far-wake is likely to be affected by external factors as well, further strengthening this argument. Based on the observations for drag reduction in unstable stratification, we propose a new expression for the drag reduction experienced by a particle settling in $\gamma_t < 0$ conditions:

$$\frac{C_D}{C_{D,0}} = 1 - \frac{Ra}{a + bRa^{1/3} + cRa^{2/3}}$$
 (2.35)

2.7 Theoretical limits for settling velocity (special case)

Following the symmetry assumption between drag enhancement and reduction under stable and unstable stratification, this investigation can be extended to settling velocity calculations. For a small sphere settling at low Reynolds numbers, the force balance can be expressed as:

$$F_{drag} = F_{gravity} - F_{buoyancy} (2.36)$$

By expanding this relationship to include both stratified and unstratified flow conditions, the corresponding settling velocities can be defined as follows.

$$u_{s} = \sqrt{\frac{4gd(\rho_{p} - \rho_{f})}{3C_{D}\rho_{f}}}, \quad \rho_{f} = \rho_{0} + \gamma z + \bar{\rho'} \quad for \ stratified \ flow$$

$$u_{s,0} = \sqrt{\frac{4gd(\rho_{p} - \rho_{f})}{3C_{D,0}\rho_{f}}}, \quad \rho_{f} = \rho_{0} \quad for \ unstratified \ flow$$

$$(2.37)$$

Here, u_s and $u_{s,0}$ denote the particle's settling velocity in stratified and unstratified conditions, respectively. For the special case where the fluid density is the same between stratified and unstratified cases, the ratio between settling velocities can be simplified to:

$$\frac{u_s}{u_{s,0}} = \sqrt{\left(\frac{C_{D,0}}{C_D}\right)} = \left[1 + \frac{Ra}{a + bRa^{1/3} + cRa^{2/3}}\right]^{-\frac{1}{2}} for \ \gamma_t > 0$$

$$\frac{u_s}{u_{s,0}} = \sqrt{\left(\frac{C_{D,0}}{C_D}\right)} = \left[1 - \frac{Ra}{a + bRa^{1/3} + cRa^{2/3}}\right]^{-\frac{1}{2}} for \ \gamma_t < 0$$
(2.38)

Using the above relationships, variations in the normalized settling velocity $(u_s/u_{s,0})$ are analyzed for the conditions of $10^{-4} < Ra < 1.5$. Assuming that the symmetry in drag behavior under stable and unstable stratification holds for $Re_p < 10$, the following plots can be generated to visualize this relationship.

Fig. 2.6 shows that particles can experience an increase to settling velocity in the presence of unstable stratification. Secondly, there is very little change in settling velocity between the cases of Re = 5 and Re = 10. These observations suggest that for Re > 5, there is a negligible change in settling velocities. As Re decreases, the change in settling velocity becomes significant. However, there appears to be an upper limit to variations in settling velocity, which is achieved at Re = 0.01. Further reductions to Re showed no noticeable difference, as evidenced by the results for Re = 0.001. Moreover, these results indicate that drag enhancement can decrease the $u_s/u_{s,0}$ ratio to 0.838, and drag reduction can increase the $u_s/u_{s,0}$ ratio to 1.314. This observation leads to the main findings of this study, which is that variations in settling velocity between $\gamma_t > 0$ (stable) and $\gamma_t < 0$ (unstable) conditions are no longer symmetric. While Fig. 2.5 shows that the drag modifications themselves are symmetric, the resulting changes in settling velocity scale with the inverse square root of the drag modification, as shown in Fig. 2.6. However, this theoretical limit is for the limiting case of similar fluid density between stratified and unstratified conditions. Furthermore, these results assume the same Re_p between stratified and unstratified conditions. Nevertheless, as demonstrated in Sec. 2.3, particles settling in stratified regions of the ocean experience both

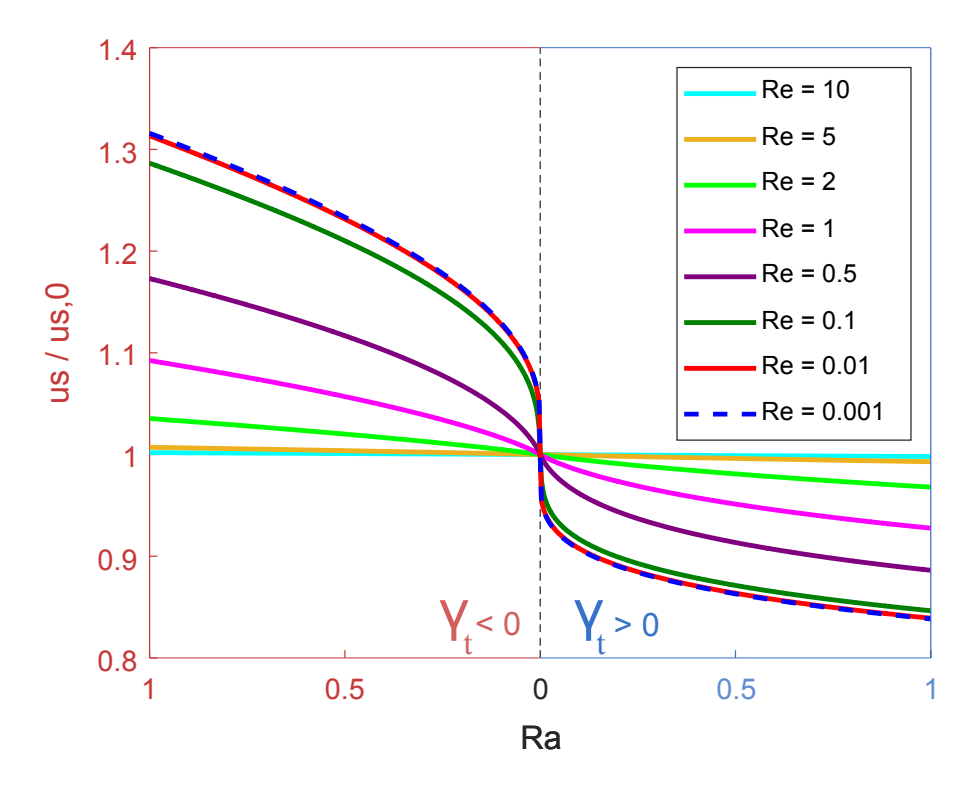


Figure 2.6: Variations in $u_s/u_{s,0}$ with Ra under the assumption that the background density between stratified and unstratified fluids is the same. This comparison highlights an asymmetry between drag enhancement and reduction.

 $\gamma_t > 0$ and $\gamma_t < 0$ conditions. The asymmetry observed in settling velocities under these two conditions could provide valuable insight into how the intermittent nature of density gradients in stratified turbulence affects the settling characteristics and collision rates of particles.

CHAPTER 3

Modeling intermediate scales

DNS is widely used as a high-fidelity tool to describe the fundamental behavior of turbulence under different environmental conditions and is given the same level of respect as experiments or field observations within the fluid mechanics community. However, the addition of DNS-derived correlations to describe particle-fluid interactions in large-scale models is rarely pursued. Additionally, it's challenging to identify the benefits of using a detailed model in large-scale simulations because the system is too dynamic. Here, the benefits of using an intermediate or transitional scale to address this problem are demonstrated. An intermediate scale modeling approach can isolate and investigate specific variables and processes while constraining environmental forcing. This enables a systematic evaluation of how they impact the fate of microplastics. The focus is on stratification (Paper 2) and biofouling (Paper 1), examining how they affect the sinking dynamics and collision rates in a turbulent environment. In stratified flows, intermittent turbulent events cause asymmetries in particle settling velocity. The importance of accounting for biofilm growth from the mean turbulent shear is demonstrated, while adding a detailed model to capture turbulence intermittency did not yield additional benefits.

3.1 Settling velocity PDF in stratified flows

The intermittency of fluctuating density gradients in the ocean can have a profound impact on the PDF of particle settling velocity. PDFs provide a statistical representation of particle settling dynamics under varying oceanographic conditions [64]. The same expressions for settling velocity stated in Eq. 2.37 are used here and coupled with the Schiller-Naumann expression for $C_{D,0}$, which is valid for rigid spherical particles settling in low Re unstratified flows [61].

$$C_{D,0} = \frac{24}{Re_p} \left(1 + 0.15 Re_p^{0.687} \right) \tag{3.1}$$

The change-of-variable approach is used for developing the PDFs of u_s . Let $u_s = g(\gamma_\rho)$ be the expression stated in Eq. 2.37 to map γ_ρ to u_s , and their corresponding PDFs to be $f_{\gamma_\rho}(\gamma_\rho)$ and $f_{u_s}(u_s)$. The following expression is valid given the monotonic relationship between u_s and γ_ρ :

$$f_{u_s}(u_s) = \left| \frac{du_s}{d\gamma_\rho} \right| \cdot f_{\gamma_\rho}(\gamma_\rho)$$
 (3.2)

where $|du_s/d\gamma_{\rho}|$ is the Jacobian of the transformation, which is numerically computed using a first-order difference approximation.

To analyze this relationship, simulations are performed for each oceanographic condition by systematically varying d and ρ_p in Eq. 2.37. The numerical constants presented in Sec. 2.2 are used for the remaining dimensional parameters in Eq. 2.37. The results demonstrate that, regardless of the ocean condition, the PDFs of u_s are governed by the maximum Rayleigh (Ra_{max}) and Reynolds (Re_{max}) numbers for the highest intermittent signal of γ_{ρ} . Fig 3.1 provides a visualization of the range in PDFs obtained during this investigation. For all cases, $d = 0.75 \ mm$, $Re_{max} \approx 1$, and ρ_p was varied such that different conditions for $\Delta \rho$ were achieved. The theoretical predictions from Fig. 2.6 are necessary to interpret the PDFs visualized in this plot. At low Ra_{max} values, the PDFs of u_s remain symmetric and non-Gaussian, as observed in the case of DO (Fig. 2.6(a)). This symmetry results from u_s increasing linearly with Ra for $Ra \ll 1$ even in extreme cases, as evident in Fig. 2.6. As Ra_{max} begins to rise, the peak observed at the mode of the PDF starts to flatten. Once $Ra_{max} \approx 1$, a flat region emerges at the center of the PDF, as observed in the EF case (Fig. 2.6(d)). This flattening occurs

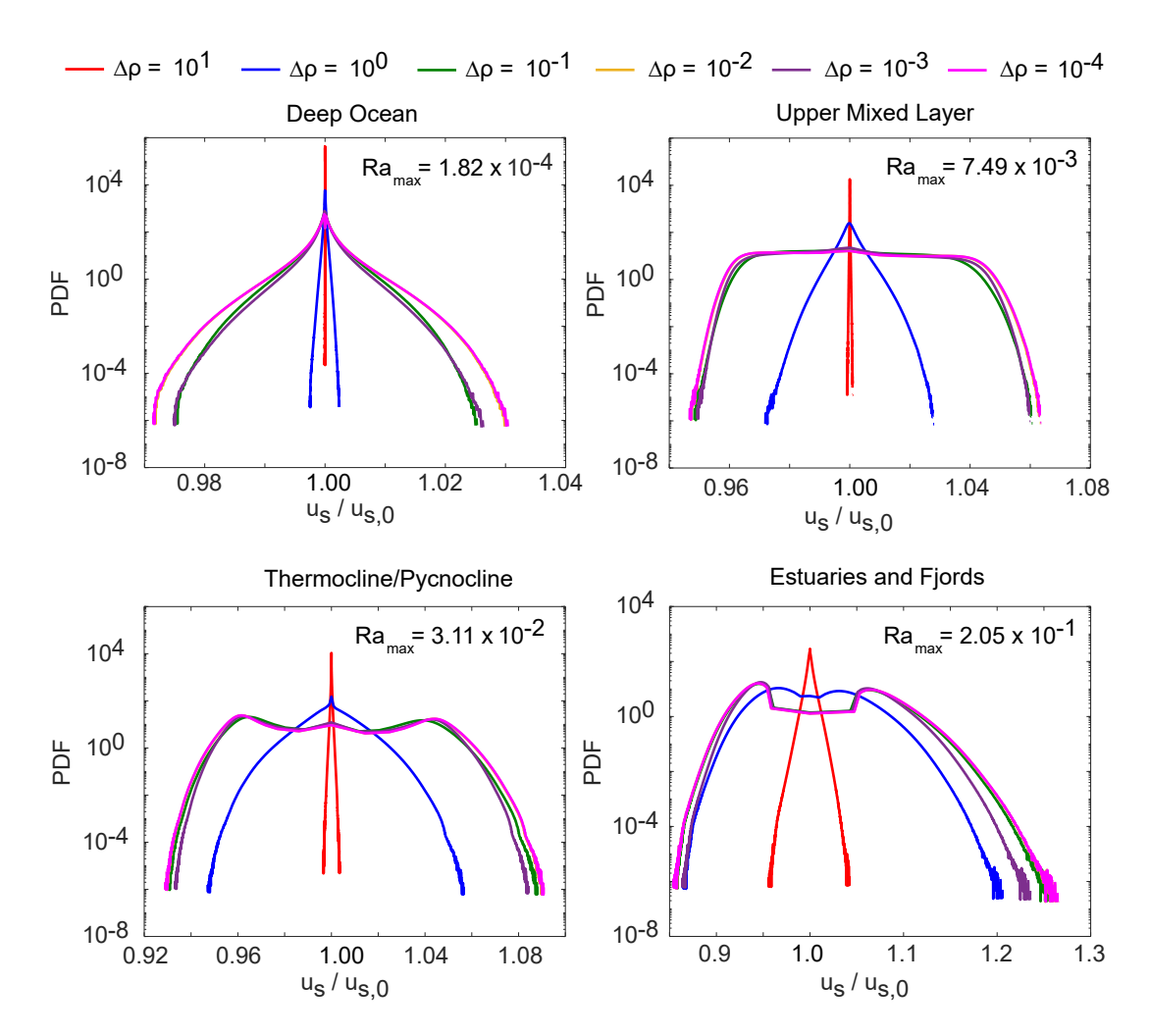


Figure 3.1: An illustration of the PDFs of settling velocity under oceanographic conditions with different strengths of stratification.

because, at very low Ra, there is an abrupt and nearly linear change in u_s for Re < 0.1. This results in a smaller range of $f_{\gamma_{\rho}}$ being mapped evenly across a broader range of u_s , leading to a flat region in $f_{u_s}(u_s)$. As Ra increases further, u_s begins to vary more gradually with Ra, resulting in a concentration of $f_{\gamma_{\rho}}(\gamma_{\rho})$ over a smaller range of u_s . This causes a sudden increase in $f_{u_s}(u_s)$ as observed with Fig. 2.6(d). The main takeaway from Fig 3.1 is the non-symmetry in PDFs of u_s as stratification effects become significant and $\Delta \rho$ becomes relatively small. In realistic ocean conditions, the fluid density surrounding a settling particle fluctuates over time due to background density gradient (γz) and density fluctuations (ρ') . Simultaneously, processes such

as biofouling cause microplastic particles to undergo gradual changes in their density. Hence, the density difference between a particle and fluid $(\Delta \rho)$ varies continuously throughout particle motion. Therefore, particles likely experience the full range of subtle and extreme flow conditions visualized in Fig 3.1. Furthermore, the increase in u_s for the case of $\gamma_\rho > 0$ (drag reduction) is more significant than the decline in u_s for the case of $\gamma_\rho > 0$ (drag enhancement). This asymmetry may have consequences for particle collision rates in the ocean, a topic that will be further investigated in the next phase of this research.

3.2 Biofouling

Large-scale numerical simulations are powerful tools for predicting the transport and fate of microplastics in the marine environment [65]. To achieve accurate predictions, such models must account for numerous physical and biological processes occurring in the ocean [66]. Due to computational limitations in resolving flow dynamics at fine spatial and temporal scales, parametrized equations represent key mechanisms such as beach wash-off, sea-floor deposition, re-suspension, degradation, and biofouling [67]. Paper 1 focuses on an intermediate scale where turbulence and biofouling are isolated and their interactions are studied. Biofouling is the accumulation of biological entities, such as algae, on the surface of microplastics [68]. This affects the buoyancy and hydrophobicity of microplastics [69]. Current estimates suggest that approximately 49% of all manufactured plastic is buoyant, yet only 1% is found on the ocean surface [70]. This suggests that biofouling may be a driving mechanism resulting in the sinking of buoyant microplastics. A novel 1D Lagrangian particle tracking (LPT) model is developed to investigate the interaction between biofouling and turbulence and how this influences the vertical motion of microplastics. The model assumes constant profiles for chlorophyll concentrations, temperature, salinity, density, and turbulent diffusivity. Turbulence mixing is parameterized using the concept of eddy diffusivity [71], while biofouling is captured using the Kooi model [72], the most detailed and widely accepted numerical framework for representing biofouling processes on microplastics. Sec. 3.3 provides more details on the numerical model.

3.3 LPT numerical setup

A brief summary of the mathematical model used in the analysis is given below. The impact of turbulence diffusion is represented using the concept of eddy diffusivity, where a K-profile parametrized expression is coupled with a random walk model to fulfill this requirement. The K-profile equation is shown below [73].

$$K(z) = \left(\frac{\kappa u_{\star w}}{\phi}\theta\right)(|z| + z_0) \left(1 - \frac{|z|}{MLD}\right)^2 \tag{3.3}$$

In Eq. 3.3, MLD is the mixed layer depth, κ is the von Kármán constant, $u_{\star w}$ is the friction velocity of the sea's surface, ϕ is the stability function of the Monin-Obukhov boundary layer theory, and θ is the Langmuir circulation enhancement factor, and z_0 is the roughness scale of turbulence. The random walk model captures the motion of microplastics in non-uniform diffusivity fields and is represented using Eqs. 3.4 and 3.5 [74], [75].

$$T_{stoc} = R \left[\frac{2K(z_n + \frac{1}{2}K'(z_n)\Delta t)}{r\Delta t} \right]^{\frac{1}{2}}$$
(3.4)

$$z_{n+1} = z_n + K'(z_n)\Delta t + T_{stoc}\Delta t + w_p\Delta t$$
(3.5)

In the above expressions, R is a normally distributed random weight with a mean of zero and a variance of r. This approach captures contributions from three components: a deterministic term representing the gradient of diffusivity (K' = dK/dz), a random term (T_{stoc}) , and an intrinsic motion term (w_p) . The deterministic term causes a net movement of particles toward regions of higher diffusivity, which is necessary to prevent particles from accumulating in areas with low diffusivity. The stochastic nature of turbulence is captured using the random term, where R is a random process with a mean of zero and a variance of r. This random number is generated based on a multiple of diffusivity but should be calculated at an offset distance of $1/2K'(z_n)\Delta t$ from the local position. Finally, the intrinsic motion term accounts for the sinking velocity of the microplastic particle, driven by the biofouling process in the present study. The biofouling rate is represented using the Kooi model, as shown in Eq. 3.6:

$$\frac{dA}{dt} = \frac{\beta_A A_A}{\gamma_{pl}} + \mu_A A - m_A A - Q_{10}^{\frac{T-20}{10}} R_A A \tag{3.6}$$

where A_A is the ambient algae concentration and γ_{pl} is the plastic particle's surface area. In Eq. 3.6, dA/dt refers to the biofouling rate, with the four terms on the right-hand side capturing contributions from: (i) collision rate between algae and microplastics (β_A) ; (ii) temperature and light-dependent algae growth (μ_A) ; losses due to (iii) algae mortality (m_A) ; and (iv) algae respiration (R_A) , respectively. One modification is made to the Kooi model to better account for turbulence-induced effects. The original Kooi model has a collision term that includes contributions from Brownian motion $(\beta_{A,Brownian})$, differential settling/sedimentation $(\beta_{A,settling})$, and constant advective shear $(\beta_{A,shear})$:

$$\beta_A = \beta_{A,Brownian} + \beta_{A,settling} + \beta_{A,shear}$$
 (3.7)

Here, the constant advective shear is replaced with a more physically representative turbulent shear term, which is detailed in Eq. 3.8.

$$\beta_{A,shear} = 1.3 \left(\frac{\epsilon_{sw,z}}{\nu_{sw,z}}\right)^{\frac{1}{2}} (r_{tot} + r_A)^3$$

$$K(z) = \Gamma\left(\frac{\epsilon_{sw,z}}{N_{bvf}^2}\right)$$

$$N_{bvf}^2 = \frac{g}{\rho_{sw,z}} \left| \left(\frac{d\rho}{dz}\right)_{sw,z} \right|$$
(3.8)

where $\epsilon_{sw,z}$ is the turbulence dissipation rate at depth z estimated using Osborn's model [76], Γ is called the efficiency factor, and N_{bvf} is the Brunt-Väisälä frequency. To capture the intermittent nature of turbulence [77], [78], Pope and Chen's stochastic turbulence dissipation model [79] is employed. This model generates a relationship for the order of magnitude of the turbulent dissipation $\chi(t) = ln(\epsilon/\bar{\epsilon})$, and represents it using an Ornstein-Uhlenbeck process, whose differential equation is shown below.

$$d\chi = -(\chi - \bar{\chi})\frac{dt}{T_{\chi}} + \left(\frac{2\sigma_{\chi}^2}{T_{\chi}}\right)^{\frac{1}{2}}dW \tag{3.9}$$

where W is a Wiener process with zero mean and variance dt, σ_{χ}^2 is the variance of $\chi(t)$ with an integral time scale of T_{χ} . Further details of this model can be found in Thisal et al. [80]. The simulations are carried out with oceanographic profiles representative of the North Pacific Ocean near Hawaii. Three common buoyant plastic types are used: Polypropylene (PP), Low-density polyethylene (LDPE), and High-density polyethylene (HDPE) with particle densities of 840 kg/m^3 , 920 kg/m^3 , and 960 kg/m^3 , respectively.

3.4 Impact of turbulence on biofouling rate

Existing research studies that employ particle tracking models for oceanographic applications often assume laminar flow or capture turbulent effects using mean values. However, turbulence is inherently intermittent, and using averaged values may lead to an inaccurate or oversimplified representation of ocean turbulence. The impact of incorporating a detailed turbulence dissipation model on the turbulent shear acting on a particle and its subsequent effects on biofilm growth is examined to address this limitation. Fig. 3.2 compares the impact of assuming mean vs fluctuating ϵ on contributions of turbulent shear towards biofouling rate.

The biofouling rate peaks at $280 \ m^{-2} s^{-1}$ for the simpler model based on mean turbulent shear. In contrast, the addition of the detailed turbulence dissipation model of Pope and Chen increased the peak value to $1897 \ m^{-2} s^{-1}$, highlighting a substantial influence of turbulence intermittency on biofilm growth for particles of $1 \ \mu m$ in size. This data corresponds to the trajectory of a single particle, demonstrating a typical intermittent signal of the shear experienced by a particle in turbulence. While the quantitative values for biofouling rate change with each particle, the qualitative behavior remains the same. For the remaining investigations, all results are averaged over a sufficiently large number of particle trajectories.

Fig. 3.3(a) investigates the contributions from shear towards biofouling rate. Fig. 3.3(b) quantifies the mean number of attached algae per unit area to provide an estimate of biofilm thickness. Comparisons are made between the

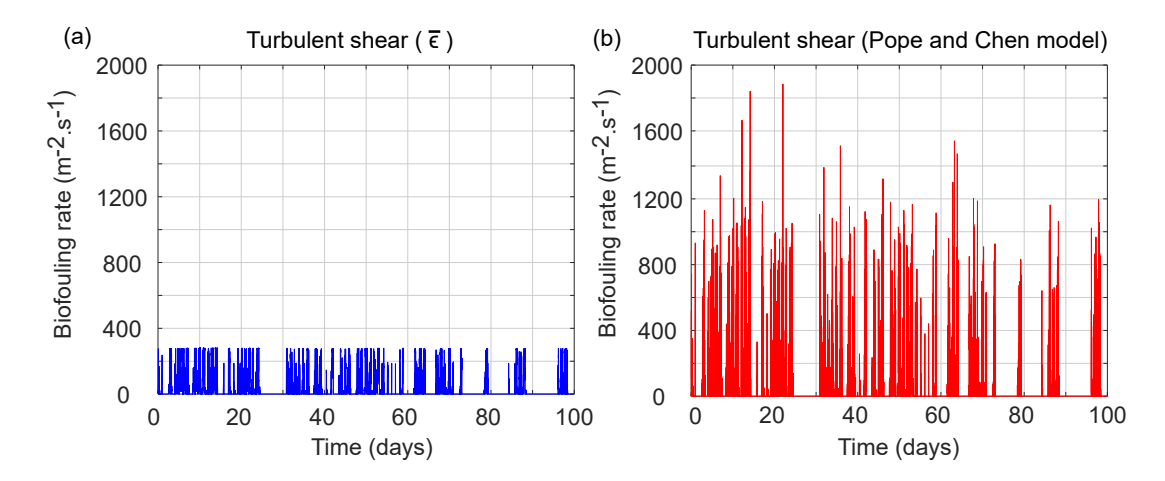


Figure 3.2: The contribution from turbulent shear towards biofouling rate for a single LDPE particle of 1 μm in size using the average dissipation $\bar{\epsilon}$ (a) and the Pope and Chen model (b).

laminar model (purple lines/symbols) and two turbulent representations: one with average dissipation $\bar{\epsilon}$ (green lines/symbols) and the Pope and Chen model (red lines/symbols). These results indicate that the constant shear assumption of the laminar model overestimates the contributions to the biofouling rate in all cases. While a significant difference is observed between the two turbulence shear models for particles larger than 0.1 mm for biofouling rates in Fig. 3.3(a), it's also shown in Fig. 3.3(b) that there is negligible difference in the biofilm thickness. Moreover, as the particle size decreases from 0.1 mm, there is a negligible difference between the two turbulence models in terms of the contributions from turbulent shear towards the biofouling rate.

Individual contributions from Eq. 3.6 are quantified and displayed in Fig. 3.4 to further investigate the influence of turbulence on the biofouling rate. These results show that for particles of size 1 mm, the contributions from growth, mortality, and respiration terms are of similar magnitude, while the contribution from collision is substantially smaller. As particle size decreases, the contributions from the collision term become more significant. More importantly, the influence of turbulent shear increases considerably. For particles smaller than 10 μm , turbulent shear becomes the dominant contributor to biofouling rate among the collision terms and is of similar magnitude to the remaining terms. However, Fig. 3.5 will demonstrate that biofouling has negligible influence on particle motion at such particle sizes.

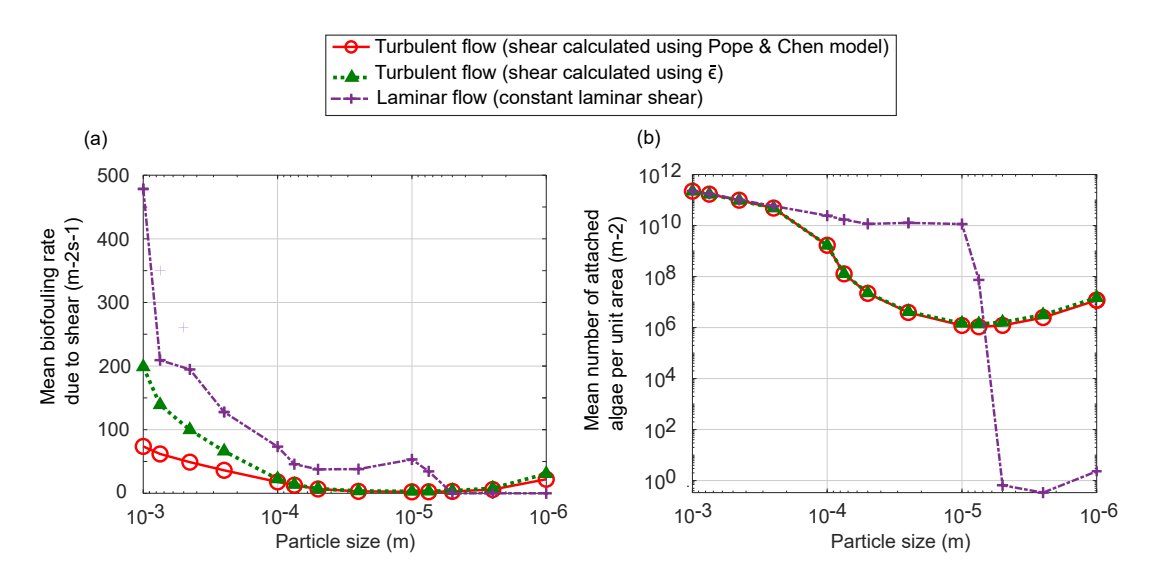


Figure 3.3: (a) Mean biofouling rate due to shear and (b) mean number of attached algae per unit area for a LDPE particle of sizes ranging from 1 mm to 1 μm .

In summary, turbulent shear contributions to the biofouling rate are negligible for larger particles but become increasingly significant for smaller sizes. However, Sec. 3.5 will show that biofouling has a negligible impact on particle trajectories at such small sizes. Consequently, it is concluded that the addition of a detailed turbulence model for biofouling rate predictions is not necessary, as the added complexity does not meaningfully affect particle motion. Moreover, implementing the detailed Pope and Chen model requires a stringent Δt of 1 s or below for numerical stability, which may not justify the computational cost.

3.5 Turbulence vs biofouling

A new plot is presented to quantify the relative importance of biofouling and turbulence for particle sizes ranging from 0.1 $\mu m \leq d \leq 5 \ mm$ and particle densities between 800 $kg/m^3 \leq \rho \leq 1000 \ kg/m^3$. The Pearson correlation coefficient (P) is used to accomplish this goal by computing a similarity index to quantify the influence of turbulence and biofouling. The expression for computing P is shown below.



Figure 3.4: The mean contributions to biofouling rate from collision, growth, mortality, and respiration observed during the last 10 days for a settling LDPE particle of (a) 1 mm (b) 0.1 mm (c) 10 μm , and (d) 1 μm in size. Error bars are provided for the different contributions.

$$P = \frac{\sum_{i=1}^{i} (z_t^i - \bar{z}_t)(z_l^i - \bar{z}_l)}{\sqrt{\sum_{i=1}^{i} (z_t^i - \bar{z}_t)(z_t^i - \bar{z}_t) \sum_{i=1}^{i} (z_l^i - \bar{z}_l)(z_l^i - \bar{z}_l)}}$$
(3.10)

In Eq. 3.10, z_t^i and z_l^i are the particle locations with respect to timestep i for a turbulent and laminar flow, while \bar{z}_t and \bar{z}_l are their respective average values. A value of P=1.0 implies that particle trajectories under turbulent and laminar conditions are proportional, suggesting that biofouling governs particle motion. On the other hand, a value of P=0.0 indicates no correlation between turbulent and laminar flow particle trajectories, implying that particles follow turbulent flow paths with negligible contributions from biofouling. The results of this analysis are displayed in Fig. 3.5.

This figure highlights several critical observations. First, particle size has a more significant impact than particle density on the vertical motion of buoyant microplastics. When biofouling is the dominant contributor to particle motion, P exceeds roughly 0.5. Such values are observed for particles larger than 0.1 mm. In Fig. 3.5, the biofouling dominant regime is visually marked by a vertical magenta line, separating it from the subsequent transitional regime. Within the transitional region, both biofouling and turbulence have a considerable impact on particle motion. As particle size decreases further, falling below approximately 8-12 μm in size, turbulent dominant conditions are achieved. This is the first contour plot developed to quantify the relative

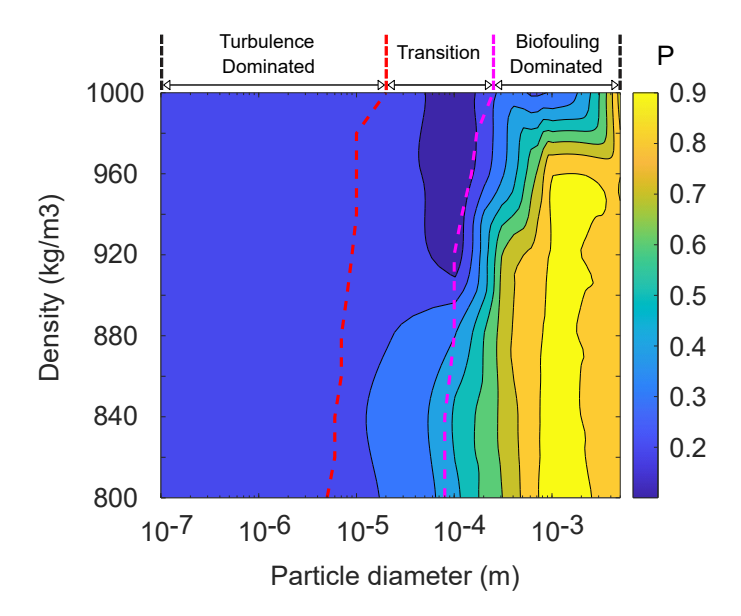


Figure 3.5: Illustration of the similarity index to highlight the influence of biofouling and turbulence on a particle's vertical motion. The magenta line indicates when the oscillatory motion of particles stops, and the red line depicts when the mean particle location reaches 50 m, indicating the transition point to the turbulence-dominated regime.

contributions of turbulence and biofouling to particle motion, specifically under conditions representative of the North Pacific Ocean. Similar plots should be generated for other marine regions to enable broader comparisons and assess how varying oceanographic conditions influence this balance. These results also have implications for tracking microplastics in large-scale numerical models. For particles smaller than $10~\mu m$, it is computationally more efficient to disable the biofilm growth model, as it has a negligible impact on the vertical motion of particles.

CHAPTER 4

Large-scale simulations

Large-scale models are traditionally used as numerical tools to provide sourceto-sink pathways of microplastics in marine environments. However, the scope of most existing studies remains limited, making it difficult to use such tools to provide detailed descriptions for environmental impact assessment. This limitation is mainly due to the lack of field data to assess the credibility of the numerical predictions. The focus here is to demonstrate the value of using numerical tools to complement field studies, explaining the fundamental mechanisms leading to observations in the field. Here lies the true potential of large-scale numerical models: not only to contextualize field data, but also to use this validation to extrapolate further unknown microplastic behaviors and potential accumulation zones that are difficult to monitor directly. A case study is carried out in the Orust-Tjörn fjord system to apply this concept to a real-world scenario. The development of a novel numerical tool, MPDrift, that is tailored to capture microplastic transport in coastal marine ecosystems is presented (Paper 3). Preliminary results reveal some similarities between numerical predictions and field observations. Mathematical descriptions of physical and biological processes, such as sediment transport and biofouling, are used to explain real-world observations and extrapolate additional details.

4.1 MPDrift

MPDrift is a Lagrangian particle tracking framework developed to study the transport of microplastics in a marine environment. It is currently being implemented as an extension to OpenDrift, an open-source software package designed to simulate the trajectories of objects drifting in the ocean. While OpenDrift provides robust tools for horizontal advection, it lacks detailed representations of the physical and biological processes governing vertical particle motion. MPDrift is being developed to fill this knowledge gap; it is specifically designed to accurately capture numerous physical and biological processes within a marine environment that affect the vertical dynamics of microplastics. MPDrift builds on established microplastic tracking models such as TrackMPD [67], [81] and CAMPSim-3D [82], and is custom-tailored for application in Swedish waters and the broader Baltic Sea region. The aim is to integrate MPDrift into environmental assessment frameworks; therefore, this goal is factored into the development stage. The end goal is to make MPDrift a platform for improving the scientific understanding of the fate of microplastics and driving policy decisions to mitigate the harmful impacts of microplastics.

4.2 Numerical framework

The mathematical model behind MPDrift is described in the following subsections. The biofouling model described in Sec. 3.3 is implemented here with additional boundary conditions. The settling velocity correction proposed by Simona et al. [83] captures the impact of irregularity in particle shape. A new model for the sediment transport of microplastics is introduced, extending the formulation by Jalón-Rojas et al. [81]. Finally, a comprehensive beaching model, initially developed for oil spill simulations [84], is planned for integration into MPDrift to more accurately represent the probability of microplastic deposition along coastlines with diverse sediment characteristics. However, the model is not detailed here as its implementation is still underway. The environmental forcing of ocean currents and wind speeds is taken from Copernicus Marine Service, and CTD profiles are obtained from Swedish Meteorological and Hydrological Institute databases.

Horizontal motion

The transport equations for horizontal motion of microplastic particles are discretized using the Euler method with a time-step of $60 \ s$. The expressions that govern particle motion in horizontal directions due to advection and diffusion are stated below.

$$x_{i+1} = x_i + U_{currents}\Delta t + U_{wind}f_w\Delta t + R[2r^{-1}K_h\Delta t]^{\frac{1}{2}}$$

$$(4.1)$$

$$y_{i+1} = y_i + V_{currents}\Delta t + V_{wind}f_w\Delta t + R[2r^{-1}K_h\Delta t]^{\frac{1}{2}}$$
 (4.2)

where x_i and y_i are the particle's initial positions, and x_{i+1} and y_{i+1} are the particle's final location, K_h is the horizontal diffusivity, $U_{currents}$ is the velocity of ocean currents, U_{wind} is the velocity of wind at a height of 10 m above the sea surface, f_w is the wind drift factor, R is a random number with a mean of zero and variance of r. The present study assumes a constant value of $1.0 \ m^2/s$ for K_h . The generated random numbers are Gaussian distributed with a mean of zero and a standard deviation of one.

Vertical motion

The expression for vertical transport is the same as Eq. 3.5, with a modification to the estimation of vertical eddy diffusivity. MPDrift currently uses the inbuilt OpenDrift model by Large et al. [85] to create the vertical diffusivity profile.

Modified settling velocity

For irregular-shaped particles in turbulent flow, where tumbling, tipping, and sliding significantly alter the sinking dynamics, the dimensionless settling velocity (w_{dim}) is calculated using the following expression:

$$w_{dim} = \frac{D_{dim}^2}{C_1 + (0.75C_2D_{dim}^3)^n}$$
(4.3)

Eq. 4.3 computes w_{dim} with respect to a reference size and shape. The reference size is represented using a reference dimensionless particle diameter

 (D_{dim}) , while the shape effects are captured using three coefficients: C_1 , C_2 , and n.

Biofouling

The biofouling model described in 3.2 is integrated into MPDrift. One additional boundary condition is implemented where the biofouling process is paused if the particles settle in the sediments of shallow regions exposed to sunlight to prevent nonphysical biofilm growth.

Sediment transport model

The sediment transport model is based on three shear stress values, bottom shear stress experienced by a particle (τ_0) , a first critical threshold for bedload transport $(\tau_{c,1})$ and a second critical threshold for resuspension into the water body $(\tau_{c,2})$. If the τ_0 experienced by a particle deposited in the sediments is lower than $\tau_{c,1}$, the particle remains deposited. If τ_0 is in between $\tau_{c,1}$ and $\tau_{c,2}$, bedload transport is activated. If τ_0 is greater than $\tau_{c,2}$, the particle is re-suspended onto the water column. This concept has been conventionally used for natural particles (Soulsby et al. [86]), and recently implemented with TrackMPD for microplastics (Jalón-Rojas et al. [81]).

4.3 Case study: Stenungsund

The potential for MPDrift to act as an environmental impact assessment tool is investigated through a case study of microplastic pollution in Stenungsund. A brief overview of the motivation for this study is initially provided, followed by a direct comparison between results from field observations and the numerical model. Finally, a summary of the insights from the biofouling and sediment transport models is provided.

Microplastic pollution

The industrial district of Stenungsund hosts one of Europe's largest polyethylene production facilities. Established in 1963, this facility has achieved an annual production output of $0.75\ Mtons$, representing around 5 % of the total polyethylene production in Europe. Stenungsund is also home to a major

polyvinyl chloride production center. In addition to production, unintended microplastic release into the environment occurs during other stages, such as handling, packaging, cleaning, and transportation, which third-party companies carry out. Fig. 4.1 illustrates an image of the plastic pellet spills recorded on the side of the road during transportation and samples of microplastics found in the sediments of Stenungsund.

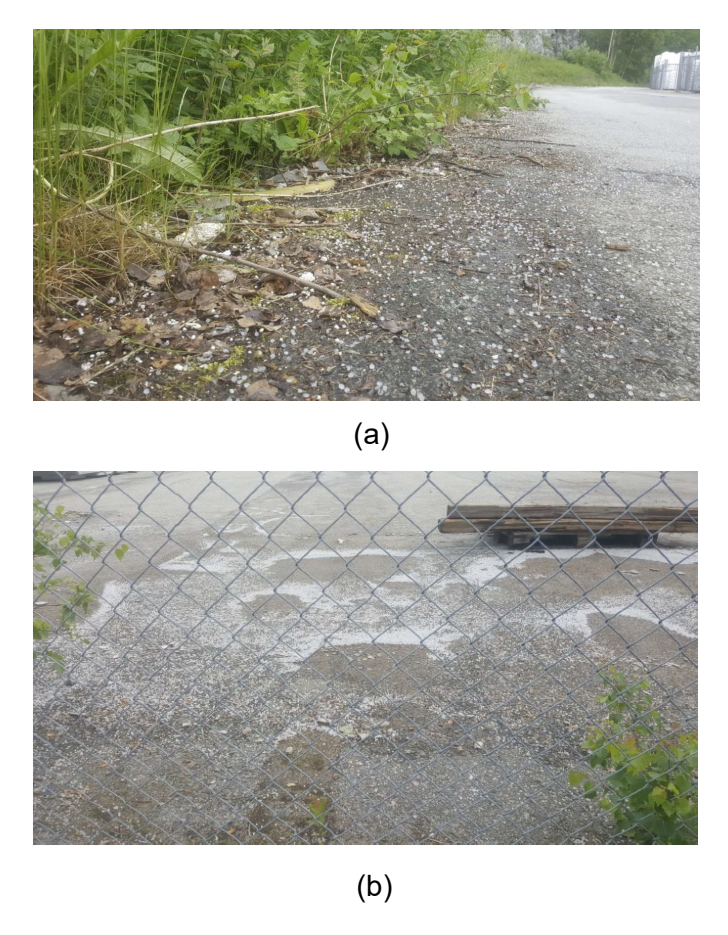


Figure 4.1: These pictures depict plastic pellet spillage observed during a field study during the year 2016 [87]. The unintended spillage has been identified to occur during transportation (a) and storage (b) in the areas surrounding Stenungsund.

Biofouling and sediment transport

Fig. 4.1 illustrates two plots, the bed shear stress experienced by a sedimented particle in January 2015 (a), and the vertical motion of a polyethylene particle

during June 2016 (b).

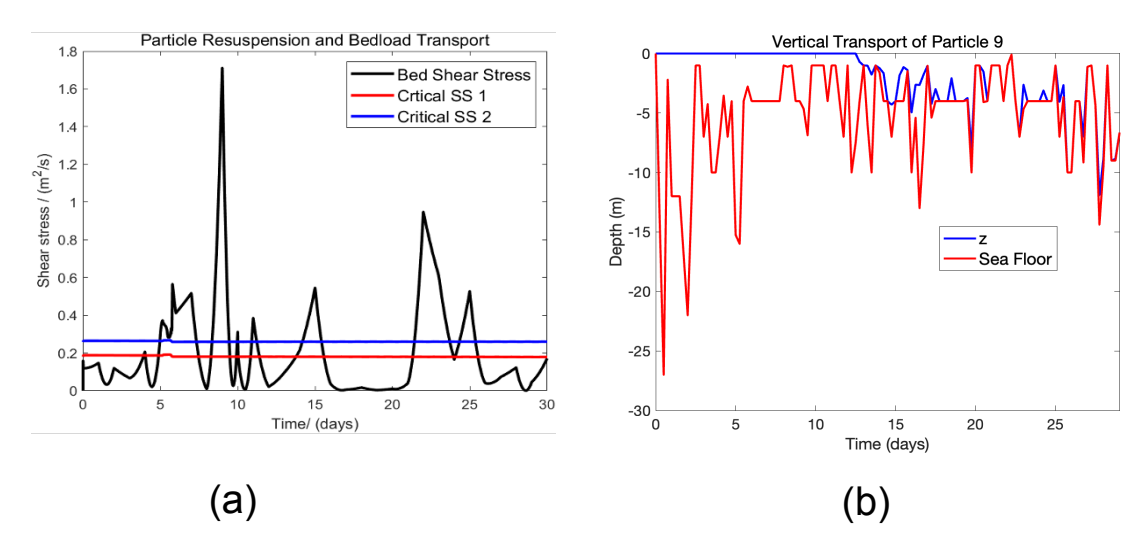


Figure 4.2: An illustration of the conceptual design of the sediment transport model (a), and the vertical motion of a polyethylene particle to demonstrate the effects of biofouling (b). In (a), the shear stress experienced by the particle is artificially multiplied by a factor of 40 to visualize the intended response of a fully developed sediment transport model. Currently, the surface currents are generally weak, leading to rare occurrences of bedload transport and particle resuspension.

Various interactions between particles and sediments can be assumed at the sea floor. When a particle collides with the sediment bed, the numerical model can consider that the particle has been deposited or buried at this location. Most existing numerical studies have assumed this interaction as a boundary condition for the model. Another approach is to allow a particle to resuspend in the presence of turbulence and bury the particle in the sediments if the residence time is sufficiently long. MPDrift employs a similar approach. A more detailed model is proposed to capture a realistic representation of particle interactions with sediments. In Fig. 4.1a, the black line represents the $40 \times \tau_0$ at the sediments of Stenungsund, the red line indicates $\tau_{c,1}$, and the blue line displays $\tau_{c,2}$. Unfortunately, during an initial simulation run for 2016, the results demonstrated that τ_0 is insufficient to initiate particle motion for a majority of the simulation period. Efforts are ongoing to identify a more suitable method for estimating τ_0 , but currently, the strength of the hydrodynamic forcing input provided by the Copernicus dataset remains relatively low for the fjords surrounding Stenungsund to initiate sediment transport. The

proposed formulation assumes a logarithmic velocity profile, which further reduces the likelihood of sediment transport. Furthermore, an additional submodel must account for burial and permanent deposition in sediments. The present simulations show particles in constant motion close to the sediments, which is physically unrealistic.

Fig. 4.1b illustrates the vertical motion of a spherical polyethylene particle, 1 mm in size, within the fjord system surrounding Stenungsund during June 2016. The particle is undergoing constant horizontal motion due to ocean currents and diffusion, causing the sea floor depth beneath the particle to change abruptly. For the first 13 days, the particle remains on the ocean surface due to buoyancy. Over time, the biofilm continues to grow until the particle density surpasses that of seawater, causing the particle to sink. From the 13^{th} day onward, the particle continuously interacts with the sea floor and resuspension events. As the sediment transport model is not activated, the resuspension is driven by turbulence diffusion. In this case, the particle trajectory hints at the potential for buoyant microplastics to spend considerable time close to the fjord sediment bed.

Fate of Polyethylene pellets

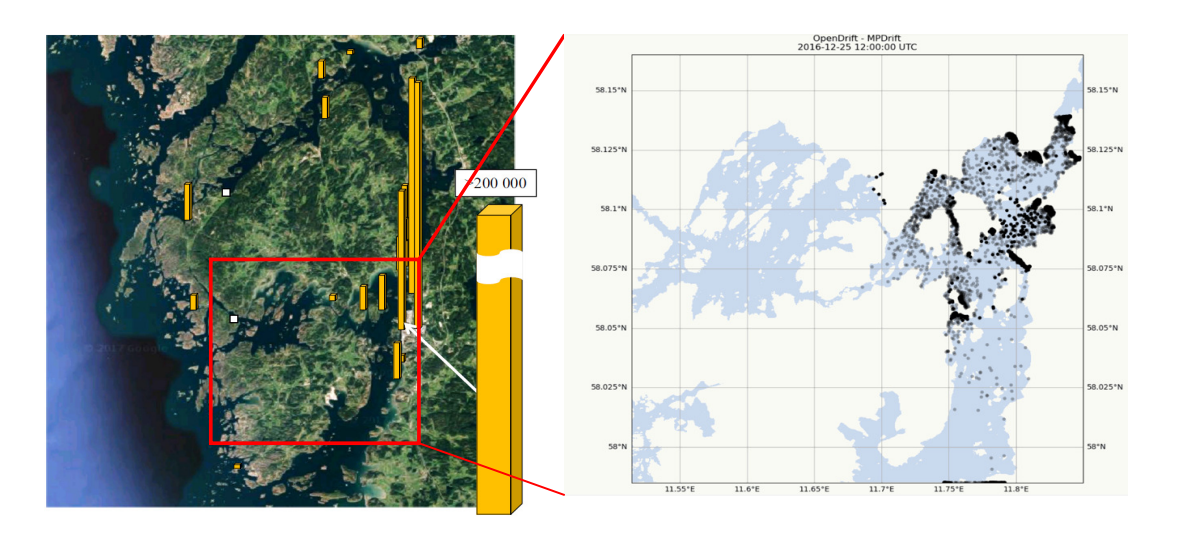


Figure 4.3: Comparisons of experimentally observed concentrations of polyethylene plastic pellets along coastal areas in Orust-Tjörn fjord system [88] with numerical predictions of MPDrift.

MPDrift is used to numerically explore the fate of polyethylene pellets released into the fjord system from Stenungsund. A significant source was identified during a 2016 field study, which estimated that approximately 1000-3000 pellets enter the fjords per hour through water pathways at Stenunge å, located in the coastal regions of Stenungsund. The simulation releases one particle per hour from Stenunge å throughout 2016, so the results can be scaled based on field observations. The results are visualized in Fig. 4.3, where a snapshot of the particle locations at the end of the simulation is presented. This simulation run does not account for beaching and uses the inbuilt sedimentation model of Open Drift. Opaque black dots indicate particles moving inside the fjord, while the translucent dots represent those deposited in the sediments. The numerical results are compared with the particle concentrations observed in the beach areas of Stenungsund during the 2016 field study. Preliminary comparisons show similarities between the modeled and observed pellet distributions along the coastal regions.

Previous research studies have highlighted the existence of a counter-clockwise net circulation in the Orust-Tjörn fjord system. The ocean currents that come through Hakefjorden enter Askeröfjord, pushing a large portion of the plastic pellets to the beach along the coastal region of Stenungsund. As a result, both observations and numerical results predict a significant amount of plastic pellets concentrated in this region. Similar concentrations of pellets are found in the Halsefjord region and the Svanesund coastal area. Furthermore, observations and the numerical model predict that a small number of particles pass through Skåpesund, between the islands of Orust and Tjörn. These pellets are expected to accumulate in the coastal region south of Svanvik. In addition to coastal deposition, the numerical model predicts that a considerable amount of pellets will be deposited on the sediments of Askerofjord and Halsefjord. However, most particles appear to settle in relatively shallow areas. One possible explanation is that the ocean currents prevent particles from remaining stationary long enough to sink to deeper parts of the fjord system. Alternatively, the biofouling process alone may be insufficient to cause sinking to such depths. These findings show the importance of validating numerical predictions with field data and highlight the value of using numerical tools to improve our understanding of the transport and fate of microplastics.

CHAPTER 5

A holistic approach to modeling marine litter transport

The investigations carried out across multiple scales are reviewed, focusing on their integration and relevance to developing predictive tools for assessing the impact of microplastic pollution in marine environments. Flow-resolving simulations have a strong potential to provide detailed physics of flow behavior and particle-fluid interactions, but struggle to deliver generalized correlations that can capture fundamental phenomena in large-scale models. Intermediate scales offer a platform to evaluate the robustness of DNS-derived correlations before implementation in large-scale models. The results presented demonstrated the benefits of constraining environmental variables to explore interactions between isolated phenomena. A new large-scale microplastic tracking model has also been developed, with a particular focus on the Baltic Sea. Microplastic pollution in Stenungsund is used as a case study to illustrate how modeling can effectively complement field studies to provide a more holistic understanding of microplastic pollution. Together, these three modeling methods form a comprehensive framework for numerically capturing the transport and fate of microplastics. Thus, this approach provides numerical simulations with the competence to join field studies in providing a holistic view of environmental pollution due to marine litter.

5.1 Micro scales

A marine environment consists of complex physical and biological processes that affect the fate of microplastics. DNS deals with physical processes and offers the most detailed method to numerically capture the underlying physics governing these processes. Its advantage lies in the ability to resolve all spatial and temporal scales of ocean turbulence, accurately capture complex oceanic phenomena such as stratification, and resolve sophisticated particle-fluid interactions. However, with the ability to provide detailed insights comes several limitations. Firstly, DNS is very computationally intensive, and the cost of resolving oceanographic conditions can scale exponentially depending on the complexity of the problem. Two such drawbacks were encountered, which include the inability to resolve stratified turbulence inside the halocline (Pr = 700) and estimate the drag experienced by particles settling in very low Re flows. For the first case, the grid resolution required to resolve stratified turbulence with pseudo-spectral DNS scales with Pr, while in the second scenario, the necessary domain size to prevent periodic boundary conditions interfering with the results is inversely proportional to Re. Furthermore, the simulation cost for the IBM method drastically increases as Re reduces. Due to this reason, hardware limitations of existing high-performance supercomputers prevent numerically exploring such scenarios. The second limitation is the requirement of mathematical descriptions for particle geometry. Consequently, DNS methods are only used to resolve the motion of spheres, oblates, prolates, and spheroids. This represents a significant obstacle for microplastics, as such particles have complex geometrical shapes, such as fragments and fibers, that cannot be mathematically described. Microplastics can also aggregate, introducing further complexities, which were represented as a combination of spheres. However, such studies are still limited to shapes with mathematical descriptions. To summarize, DNS methods describe how flow structures and particle-fluid interactions occur at a fundamental level, which, in the case of microplastics, provides all the necessary details of physical processes in the ocean that will affect the transport and ultimate fate. Significant advancements have occurred in the past few decades in applying DNS to capture the complex nature of ocean turbulence. However, there remains an urgent need to develop effective parameterizations that can translate these detailed findings into large-scale models for simulating the transport and fate of marine litter.

5.2 Intermediate scales

Studies on intermediate scales are necessary for bridging the gap between flowresolved simulations in the small scales and large-scale oceanographic models. The scientific community often underestimates the importance of this scale, where the focus tends to lie either on highly detailed simulations that resolve microscale dynamics or large-scale models driven by environmental forcing to capture real-world oceanic conditions. A wall currently exists that prevents the results of fully resolved simulations from being used in large-scale simulations, causing a loss of information when scaling up to large-scale models. Most large-scale models rely on empirical correlations developed using laboratory experiments and field observations to define particle behavior, capturing only "mean" dynamics in turbulent environments. However, turbulence is inherently intermittent and spatially heterogeneous, and relying solely on mean flow statistics can lead to oversimplified representations and inaccurate numerical predictions. The primary argument for using mean-flow assumptions is that capturing fine-scale turbulent statistics requires a temporal or spatial resolution that is computationally impractical for large-scale simulations, while providing limited benefits. Additionally, large-scale models include many dynamic components, making it difficult to quantify the importance of accounting for turbulence statistics. Investigations in the intermediate scales solve this limitation by constraining environment complexities and isolating specific variables. Such an approach allows for a systematic evaluation of how different levels of turbulent information can affect particular processes that influence the fate of microplastics. As shown here, intermediate-scale investigations could lead to unsatisfactory results, as in the case of the influence of turbulence on the biofouling process. While the Pope and Chen dissipation model proved effective in capturing intermittent turbulence statistics, its influence on the biofouling process had a negligible impact on particle settling dynamics. However, the Pope and Chen model may hold more significant potential for accurately capturing other physical and biological processes in a marine ecosystem. Turbulence can also induce asymmetrical behavior of key parameters in the ocean, such as density gradients with stratified flows. Such asymmetries, including settling velocities, can significantly alter particle dynamics. The resulting highly non-Gaussian and asymmetric statistics of settling velocities may, under certain oceanographic conditions, influence aggregation and collision processes in ways not previously captured, offering

new insights into the fate and transport of microplastics. These studies are carried out at an intermediate scale, further emphasizing their role within a multi-scale modeling framework for microplastics.

5.3 Large scales

Large-scale models have historically excelled at capturing fundamental processes within a marine environment that contribute to microplastic transport and provide source-to-sink pathways that determine their fate. Due to the dynamic nature of these aquatic ecosystems, flow variables such as temperature, salinity, chlorophyll concentration, turbulence diffusivity, ocean currents, and wind speed vary significantly over time and space. In addition, microplastic particles have different shapes and sizes, ranging from fragments to fibers, influencing their vertical and horizontal transport dynamics. Despite growing interest, limited field data that captures the full spectrum of variables across diverse marine regions is available. Consequently, existing large-scale numerical studies have focused on assessing the sensitivity of microplastic fate to variations in environmental drivers, rather than exploring the broader environmental applicability of such numerical tools. This disconnect has caused a lack of confidence among field researchers regarding the reliability of modeling tools to consistently explain observed microplastic behaviors in real-world marine environments.

The present study employs a holistic approach to solve this problem, combining numerical predictions with field observations to explain the **State** of a marine environment that governs the fate of microplastics. Over the past decade, field studies have identified Stenungsund as a hotspot for microplastic discharge to the surrounding fjord system. Due to **Drivers** such as growing industrial needs, plastic production facilities have been established in the chemical industry of Stenungsund in the 1960s and have since produced substantial quantities of plastic pellets, commonly referred to as microplastics. In addition to production, various human **Activities** such as packaging, transport, and cleaning, are conducted by third-party entities that directly involve microplastics. Due to mishandling and operational negligence, considerable microplastics have leaked into the environment and ultimately entered the fjord system (**Pressures**). Estimates in 2016 suggest that discharge rates could be as high as 1000 - 3000 particles per hour.

The **State** of the Orust-Tjörn fjord system, which includes physical, biological, and chemical parameters, has been extensively monitored over several years, with data made publicly available by the Swedish Meteorological and Hydrological Institute. Additional environmental forcings, such as ocean currents and wind speeds, are freely accessible via the Copernicus Marine Service. The **Impacts** of microplastics have been studied and published by experts within this field, leading to **Responses** such as new policies and mitigation strategies by the European Union to prevent plastic pellets from leaking into the environment at every stage of the supply chain. The case study thus represents a complete application of the DAPSIR framework. A modeling study was conducted to investigate the role of large-scale numerical simulations within this context. The simulation setup uses a microplastic source identified during field surveys, and the model includes as many details as possible from the publicly available data on the **State** of the surrounding fjord system. The following conclusions were drawn based on the results.

- 1. Large-scale numerical models have tremendous potential to explain the fundamental mechanisms leading to observations of microplastic pollution in the real world.
- 2. However, there is still ambiguity among the many sub-models representing oceanic processes such as biofouling, beaching, and sediment transport. Further model validation through experimental studies is necessary to improve the accuracy.
- 3. Large-scale models excel at providing a complete picture of the fate of microplastics in marine environments that are difficult to assess with only field studies.
- 4. These models can guide the design of future monitoring strategies by identifying potential accumulation hotspots.
- 5. They serve as powerful visualization tools for communicating scientific findings to policymakers, regulators, and the general public.
- 6. While it is difficult for numerical models to provide direct policy recommendations, they can be used to evaluate the effectiveness of mitigation strategies.

To summarize, large-scale models complement field studies and regulatory initiatives in providing a foundation for environmental impact assessment of microplastic pollution. They represent an irreplaceable component of the broader effort to understand and mitigate microplastic contamination, offering unique insights that other approaches cannot fully substitute. It is therefore concluded that numerical models will play a vital role in addressing microplastic pollution for many years to come.

CHAPTER 6

Concluding Remarks and Future Work

Numerical models are essential tools for advancing our understanding of microplastic pollution. However, the marine environment consists of numerous fundamental phenomena and processes that operate at vastly different spatial and temporal scales, making it impossible for a single modeling approach to capture all the relevant physics influencing the transport and fate of microplastics. A multi-scaling modeling strategy is proposed to address this limitation, combining flow-resolving simulations with large-scale particle tracking models. An intermediate modeling scale is introduced to bridge these two ends, enabling a complete representation of the full range of physical processes.

Each of these modeling approaches has a different role within this framework. Flow-resolving methods are tasked with investigating the fundamental mechanisms of flow phenomena, mixing events, and particle-fluid interactions under complex oceanographic conditions. Large-scale simulations, by contrast, incorporate environmental processes to explain observed patterns of microplastic contamination in the field. Intermediate scale modeling is introduced to bridge these two modeling methods. It acts as a platform to test DNS-derived correlations and isolate variables and processes in the ocean to investigate how they interact and govern microplastic transport.

For the remainder of this thesis project, further studies will be carried out on developing and applying a multi-scale modeling framework to design numerical tools for environmental impact assessment. The main objectives include advancing MPDrift, parameterizing stratification effects, and creating a model to evaluate interactions between ship-wake-induced turbulence and microplastic transport. Planned MPDrift extensions include a beaching model, an accurate vertical diffusivity model for Stenungsund, a stratification model, and a particle degradation model. Parameterizing the mixing effects of stratified turbulence poses a significant challenge and will be further explored in detail. The shipping industry also contributes to microplastic discharge into the ocean. Sources include the presence of microplastics in grey water, leakages from mishandling during transport of plastic pellets, and the breakup of anti-fouling paint used on a ship's hull with microplastics as a primary adhesive component. The interaction of microplastics with the ship wake will be simulated to quantify the potential of ship-wake-induced mixing to promote particle retention on the ocean surface.

References

- [1] United Nations Environment Programme, Drowning in plastics marine litter and plastic waste vital graphics, 2021.
- [2] J. Montoya, "Europe's plastics industry in 2023," *Plastics Engineering*, 2024, Accessed: April 25, 2025.
- [3] V. P. Sharma, R. L. Singh, and R. P. Singh, "Degradable polymers and plastics of the future: Steps toward environmental sustainability, regulations, and safety aspects," in *Principles and Applications of Environmental Biotechnology for a Sustainable Future*, R. L. Singh, Ed. Springer Singapore, 2017, pp. 467–487, ISBN: 978-981-10-1866-4.
- [4] P. Skoczinski, M. Carus, G. Tweddle, et al., Bio-based Building Blocks and Polymers Global Capacities, Production and Trends 2022–2027. Hürth, Germany: nova-Institut GmbH, 2023.
- [5] M. Cole, P. Lindeque, C. Halsband, and T. S. Galloway, "Microplastics as contaminants in the marine environment: A review," *Marine Pollution Bulletin*, vol. 62, no. 12, pp. 2588–2597, 2011, ISSN: 0025-326X.
- [6] S. Borrelle, J. Ringma, K. Lavender Law, et al., "Predicted growth in plastic waste exceeds efforts to mitigate plastic pollution," Science, vol. 369, no. 6509, pp. 1515–1518, 2020, ISSN: 0036-8075.
- [7] N. B. Hartmann, T. Hüffer, R. C. Thompson, et al., "Are we speaking the same language? recommendations for a definition and categorization framework for plastic debris," *Environmental Science & Technology*, vol. 53, no. 3, pp. 1039–1047, 2019.

- [8] K. Ziani, C.-B. Ioniță-Mîndrican, M. Mititelu, et al., "Microplastics: A real global threat for environment and food safety: A state of the art review," *Nutrients*, vol. 15, no. 3, p. 617, 2023.
- [9] A. L. Andrady, "Weathering and fragmentation of plastic debris in the ocean environment," *Marine Pollution Bulletin*, vol. 180, p. 113761, 2022, ISSN: 0025-326X.
- [10] H. Zhang, "Transport of microplastics in coastal seas," *Estuarine, Coastal and Shelf Science*, vol. 199, pp. 74–86, 2017, ISSN: 0272-7714.
- [11] Á. Borja, M. Elliott, J. Carstensen, A.-S. Heiskanen, and W. van de Bund, "Marine management towards an integrated implementation of the european marine strategy framework and the water framework directives," *Marine Pollution Bulletin*, vol. 60, no. 12, pp. 2175–2186, 2010, ISSN: 0025-326X.
- [12] J. P. Atkins, D. Burdon, M. Elliott, and A. J. Gregory, "Management of the marine environment: Integrating ecosystem services and societal benefits with the dpsir framework in a systems approach," *Marine Pollution Bulletin*, vol. 62, no. 2, pp. 215–226, 2011, ISSN: 0025-326X.
- [13] OSPAR Commission, OSPAR Quality Status Report 2023, Online, Available at: https://oap.ospar.org/en/ospar-assessments/quality-status-reports/qsr-2023/qsr2023-reference/, OSPAR Commission, 2023.
- [14] M. N. Miranda, A. M. Silva, and M. F. R. Pereira, "Microplastics in the environment: A dpsir analysis with focus on the responses," *Science of The Total Environment*, vol. 718, p. 134 968, 2020, ISSN: 0048-9697.
- [15] E. Commission, S. CEU, D.-G. for Research, and Innovation, *Microplastic pollution The policy context Background paper*. Publications Office, 2018.
- [16] European Parliament and Council of the European Union, Directive 2008/56/ec establishing a framework for community action in the field of marine environmental policy (marine strategy framework directive), Accessed: April 25, 2025, 2008.

- [17] European Parliament and Council of the European Union, Commission Decision (EU) 2017/848 of 17 May 2017 laying down criteria and methodological standards on good environmental status of marine waters and specifications and standardised methods for monitoring and assessment. European Union, 2017, vol. L 125, pp. 43-74, https://eurlex.europa.eu/legal-content/EN/TXT/?uri=CELEX:32017D0848.
- [18] N. Prinz and Š. Korez, "Understanding how microplastics affect marine biota on the cellular level is important for assessing ecosystem function: A review," in Springer International Publishing, 2020, pp. 101–120, ISBN: 978-3-030-20389-4.
- [19] S. B. Sjollema, P. Redondo-Hasselerharm, H. A. Leslie, M. H. Kraak, and A. D. Vethaak, "Do plastic particles affect microalgal photosynthesis and growth?" *Aquatic Toxicology*, vol. 170, pp. 259–261, 2016, ISSN: 0166-445X.
- [20] N. Khalid, M. Aqeel, A. Noman, S. M. Khan, and N. Akhter, "Interactions and effects of microplastics with heavy metals in aquatic and terrestrial environments," *Environmental Pollution*, vol. 290, p. 118 104, 2021, ISSN: 0269-7491.
- [21] W. Mei, G. Chen, J. Bao, M. Song, Y. Li, and C. Luo, "Interactions between microplastics and organic compounds in aquatic environments: A mini review," *Science of The Total Environment*, vol. 736, p. 139472, 2020, ISSN: 0048-9697.
- [22] G. Caruso, "Microplastics as vectors of contaminants," *Marine Pollution Bulletin*, vol. 146, pp. 921–924, 2019.
- [23] Council of the European Union, Plastic pellet losses: Council and parliament agree on new rules to reduce microplastic pollution, Accessed: 3 May 2025, 2025.
- [24] S. Zhao, K. F. Kvale, L. Zhu, et al., "The distribution of subsurface microplastics in the ocean," *Nature*, vol. 641, pp. 51–61, 2025.
- [25] P. Garaud, G. P. Chini, L. Cope, K. Shah, and C.-c. P. Caulfield, "Numerical validation of scaling laws for stratified turbulence," *Journal of Fluid Mechanics*, vol. 991, R1, 2024.

- [26] A. Doostmohammadi, R. Stocker, and A. M. Ardekani, "Low-reynolds-number swimming at pycnoclines," *Proceedings of the National Academy of Sciences*, vol. 109, no. 10, pp. 3856–3861, 2012.
- [27] R. V. More and A. M. Ardekani, "Motion in stratified fluids," *Annual Review of Fluid Mechanics*, vol. 55, pp. 157–192, 2023.
- [28] M. Bigdeli, A. Mohammadian, A. Pilechi, and M. Taheri, "Lagrangian modeling of marine microplastics fate and transport: The state of the science," *Journal of Marine Science and Engineering*, vol. 10, no. 4, 2022, ISSN: 2077-1312.
- [29] E. van Sebille, S. M. Griffies, R. Abernathey, et al., "Lagrangian ocean analysis: Fundamentals and practices," Ocean Modelling, vol. 121, pp. 49–75, 2018, ISSN: 1463-5003.
- [30] T. Dauxois, T. Peacock, P. Bauer, et al., "Confronting grand challenges in environmental fluid mechanics," Phys. Rev. Fluids, vol. 6, p. 020501, 2 Feb. 2021.
- [31] I. Ruvalcaba Baroni, E. Almroth-Rosell, L. Axell, et al., "Validation of the coupled physical-biogeochemical ocean model nemo-scobi for the north sea-baltic sea system," Biogeosciences, vol. 21, no. 8, pp. 2087–2132, 2024.
- [32] J. R. Farmer, D. M. Sigman, J. Granger, et al., "Arctic ocean stratification set by sea level and freshwater inputs since the last ice age," Nature Geoscience, vol. 14, no. 9, pp. 684–689, 2021.
- [33] G. Li, L. Cheng, J. Zhu, et al., "Increasing ocean stratification over the past half-century," Nature Climate Change, vol. 10, no. 12, pp. 1116–1123, 2020.
- [34] Z. Ljubešić, H. Mihanović, A. Matek, et al., "Marine plankton community and net primary production responding to island-trapped waves in a stratified oligotrophic ecosystem," *Heliyon*, vol. 10, no. 18, e37788, 2024, ISSN: 2405-8440.
- [35] R. M. Holmes, J. D. Zika, and M. H. England, "Diathermal heat transport in a global ocean model," *Journal of Physical Oceanography*, vol. 49, no. 1, pp. 141–161, 2019.

- [36] S. Ahmerkamp, B. Liu, K. Kindler, et al., "Settling of highly porous and impermeable particles in linear stratification: Implications for marine aggregates," *Journal of Fluid Mechanics*, vol. 931, A9, 2022.
- [37] R. Mehaddi, F. Candelier, and B. Mehlig, "Inertial drag on a sphere settling in a stratified fluid," *Journal of Fluid Mechanics*, vol. 855, pp. 1074–1087, 2018.
- [38] E. Uurasjärvi, M. Pääkkönen, O. Setälä, A. Koistinen, and M. Lehtiniemi, "Microplastics accumulate to thin layers in the stratified baltic sea," *Environmental Pollution*, vol. 268, p. 115 700, 2021, ISSN: 0269-7491.
- [39] S. MacIntyre, A. L. Alldredge, and C. C. Gotschalk, "Accumulation of marines now at density discontinuities in the water column," *Limnology and Oceanography*, vol. 40, no. 3, pp. 449–468, 1995.
- [40] A. M. Ardekani, A. Doostmohammadi, and N. Desai, "Transport of particles, drops, and small organisms in density stratified fluids," *Phys. Rev. Fluids*, vol. 2, p. 100503, 10 Oct. 2017.
- [41] A. M. Ardekani and R. Stocker, "Stratlets: Low reynolds number pointforce solutions in a stratified fluid," *Phys. Rev. Lett.*, vol. 105, p. 084 502, 8 Aug. 2010.
- [42] H. Xu, C. D. Cantwell, C. Monteserin, C. Eskilsson, A. P. Engsig-Karup, and S. J. Sherwin, "Spectral/hp element methods: Recent developments, applications, and perspectives," *Journal of Hydrodynamics*, vol. 30, no. 1, pp. 1–22, 2018.
- [43] G. BRETHOUWER, P. BILLANT, E. LINDBORG, and J.-M. CHOMAZ, "Scaling analysis and simulation of strongly stratified turbulent flows," *Journal of Fluid Mechanics*, vol. 585, pp. 343–368, 2007.
- [44] S. A. Thorpe, *The Turbulent Ocean*. Cambridge University Press, 2005.
- [45] M. C. Gregg, "Scaling turbulent dissipation in the thermocline," *Journal of Geophysical Research: Oceans*, vol. 94, no. C7, pp. 9686–9698, 1989.
- [46] P. C. Chu and C. Fan., "Global climatological data of ocean thermohaline parameters derived from woa18," *Scientific data*, vol. 10, no. 408, 1 2023.

- [47] C. Marchioli, H. Bhatia, G. Sardina, L. Brandt, and A. Soldati, "Role of large-scale advection and small-scale turbulence on vertical migration of gyrotactic swimmers," *Phys. Rev. Fluids*, vol. 4, p. 124304, 12 Dec. 2019.
- [48] K. L. Polzin, J. M. Toole, J. R. Ledwell, and R. W. Schmitt, "Spatial variability of turbulent mixing in the abyssal ocean," *Science*, vol. 276, no. 5309, pp. 93–96, 1997.
- [49] M. Rogerson, G. R. Bigg, E. J. Rohling, and J. Ramirez, "Vertical density gradient in the eastern north atlantic during the last 30,000 years," *Climate Dynamics*, vol. 39, no. 3-4, pp. 589–598, 2012.
- [50] H. van Haren, G. Voet, M. H. Alford, and D. J. Torres, "Internal wave breaking near the foot of a steep east-pacific continental slope," *Progress in Oceanography*, vol. 205, p. 102817, 2022, ISSN: 0079-6611.
- [51] D. G. MacDonald and W. R. Geyer, "Turbulent energy production and entrainment at a highly stratified estuarine front," *Journal of Geophysical Research: Oceans*, vol. 109, no. C5, 2004.
- [52] H. Peters, "Spatial and temporal variability of turbulent mixing in an estuary," *Journal of Marine Research*, vol. 57, no. 6, pp. 805–845, 1999.
- [53] H. L. Grant, R. W. Stewart, and A. Moilliet, "Turbulence spectra from a tidal channel," *Journal of Fluid Mechanics*, vol. 12, no. 2, pp. 241–268, 1962.
- [54] J.-B. Sallée, V. Pellichero, C. Akhoudas, et al., "Summertime increases in upper-ocean stratification and mixed-layer depth," *Nature*, vol. 591, pp. 592–598, 2021.
- [55] M. H. Sharqawy, J. H. L. V, and S. M. Zubair, "Thermophysical properties of seawater: A review of existing correlations and data," *Desalination and Water Treatment*, vol. 16, pp. 354–380, 2010.
- [56] K. G. Nayar, M. H. Sharqawy, L. D. Banchik, and J. H. L. V, "Thermophysical properties of seawater: A review and new correlations that include pressure dependence," *Desalination*, vol. 390, pp. 1–24, 2016.
- [57] S. M. de Bruyn Kops, "Classical scaling and intermittency in strongly stratified boussinesq turbulence," *Journal of Fluid Mechanics*, vol. 775, pp. 436–463, 2015.

- [58] W.-P. Breugem, "A second-order accurate immersed boundary method for fully resolved simulations of particle-laden flows," *Journal of Computational Physics*, vol. 231, no. 13, pp. 4469–4498, 2012, ISSN: 0021-9991.
- [59] R. V. More, M. N. Ardekani, L. Brandt, and A. M. Ardekani, "Orientation instability of settling spheroids in a linearly density-stratified fluid," *Journal of Fluid Mechanics*, vol. 929, A7, 2021.
- [60] M. Niazi Ardekani, O. Abouali, F. Picano, and L. Brandt, "Heat transfer in laminar couette flow laden with rigid spherical particles," *Journal of Fluid Mechanics*, vol. 834, pp. 308–334, 2018.
- [61] H. Lee, I. Fouxon, and C. Lee, "Sedimentation of a small sphere in stratified fluid," *Phys. Rev. Fluids*, vol. 4, p. 104 101, 10 Oct. 2019.
- [62] G. Lupo, M. Niazi Ardekani, L. Brandt, and C. Duwig, "An immersed boundary method for flows with evaporating droplets," *International Journal of Heat and Mass Transfer*, vol. 143, p. 118563, 2019, ISSN: 0017-9310.
- [63] A. Doostmohammadi, S. Dabiri, and A. M. Ardekani, "A numerical study of the dynamics of a particle settling at moderate reynolds numbers in a linearly stratified fluid," *Journal of Fluid Mechanics*, vol. 750, pp. 5–32, 2014.
- [64] A. Maffioli, "Asymmetry of vertical buoyancy gradient in stratified turbulence," *Journal of Fluid Mechanics*, vol. 870, pp. 266–289, 2019.
- [65] J. T. Potemra, "Numerical modeling with application to tracking marine debris," *Marine Pollution Bulletin*, vol. 65, no. 1, pp. 42–50, 2012, ISSN: 0025-326X.
- [66] A. Shamskhany and S. Karimpour, "The role of microplastics' size and density on their vertical turbulent mixing and transport," in *Proceedings* of the Canadian Society of Civil Engineering Annual Conference 2021, Singapore: Springer Nature Singapore, 2022, pp. 253–265, ISBN: 978-981-19-1065-4.
- [67] I. Jalón-Rojas, X. H. Wang, and E. Fredj, "A 3d numerical model to track marine plastic debris (trackmpd): Sensitivity of microplastic trajectories and fates to particle dynamical properties and physical processes," *Marine Pollution Bulletin*, vol. 141, pp. 256–272, 2019, ISSN: 0025-326X.

- [68] M. Van Melkebeke, C. Janssen, and S. De Meester, "Characteristics and sinking behavior of typical microplastics including the potential effect of biofouling: Implications for remediation," *Environmental Science & Technology*, vol. 54, no. 14, pp. 8668–8680, 2020.
- [69] D. Kaiser, N. Kowalski, and J. J. Waniek, "Effects of biofouling on the sinking behavior of microplastics," *Environmental Research Letters*, vol. 12, p. 124 003, Nov. 2017.
- [70] A. Cózar, F. Echevarría, J. I. González-Gordillo, et al., "Plastic debris in the open ocean," *Proceedings of the National Academy of Sciences*, vol. 111, no. 28, pp. 10239–10244, 2014.
- [71] R. Fischer, D. Lobelle, M. Kooi, et al., "Modelling submerged biofouled microplastics and their vertical trajectories," *Biogeosciences*, vol. 19, no. 8, pp. 2211–2234, 2022.
- [72] M. Kooi, E. H. v. Nes, M. Scheffer, and A. A. Koelmans, "Ups and downs in the ocean: Effects of biofouling on vertical transport of microplastics," Environmental Science & Technology, vol. 51, no. 14, pp. 7963–7971, 2017.
- [73] M. Boufadel, R. Liu, L. Zhao, et al., "Transport of oil droplets in the upper ocean: Impact of the eddy diffusivity," Journal of Geophysical Research: Oceans, vol. 125, no. 2, 2020.
- [74] A. W. Visser, "Using random walk models to simulate the vertical distribution of particles in a turbulent water column," *Marine Ecology Progress Series*, vol. 158, pp. 275–281, 1997.
- [75] J. Hunter, P. Craig, and H. Phillips, "On the use of random walk models with spatially variable diffusivity," *Journal of Computational Physics*, vol. 106, no. 2, pp. 366–376, 1993, ISSN: 0021-9991.
- [76] T. R. Osborn, "Estimates of the local rate of vertical diffusion from dissipation measurements," *Journal of Physical Oceanography*, vol. 10, no. 1, pp. 83–89, 1980.
- [77] R. Watteaux, G. Sardina, L. Brandt, and D. Iudicone, "On the time scales and structure of lagrangian intermittency in homogeneous isotropic turbulence," *Journal of Fluid Mechanics*, vol. 867, pp. 438–481, 2019.

- [78] J. Isern-Fontanet and A. Turiel, "On the connection between intermittency and dissipation in ocean turbulence: A multifractal approach," *Journal of Physical Oceanography*, vol. 51, no. 8, pp. 2639–2653, 2021.
- [79] S. B. Pope and Y. L. Chen, "The velocity-dissipation probability density function model for turbulent flows," *Physics of Fluids A: Fluid Dynamics*, vol. 2, no. 8, pp. 1437–1449, Aug. 1990, ISSN: 0899-8213.
- [80] T. M. Sugathapala, T. Capuano, L. Brandt, D. Iudicone, and G. Sardina, "Vertical transport of buoyant microplastic particles in the ocean: The role of turbulence and biofouling," *Environmental Pollution*, vol. 369, p. 125 819, 2025, ISSN: 0269-7491.
- [81] I. Jalón-Rojas, D. Sous, and V. Marieu, "A wave-resolving two-dimensional vertical lagrangian approach to model microplastic transport in nearshore waters based on trackmpd 3.0," *Geoscientific Model Development*, vol. 18, no. 2, pp. 319–336, 2025.
- [82] A. Pilechi, A. Mohammadian, and E. Murphy, "A numerical framework for modeling fate and transport of microplastics in inland and coastal waters," *Marine Pollution Bulletin*, vol. 184, p. 114119, 2022, ISSN: 0025-326X.
- [83] S. Francalanci, E. Paris, and L. Solari, "On the prediction of settling velocity for plastic particles of different shapes," *Environmental Pollution*, vol. 290, p. 118 068, 2021.
- [84] A. G. Samaras, M. De Dominicis, R. Archetti, A. Lamberti, and N. Pinardi, "Towards improving the representation of beaching in oil spill models: A case study," *Marine Pollution Bulletin*, vol. 88, no. 1–2, pp. 91–101, 2014.
- [85] W. G. Large, J. C. McWilliams, and S. C. Doney, "Oceanic vertical mixing: A review and a model with a nonlocal boundary layer parameterization," *Reviews of Geophysics*, vol. 32, no. 4, pp. 363–403, 1994.
- [86] R. Soulsby, Dynamics of Marine Sands: A Manual for Practical Applications. ICE Publishing, 1997, ISBN: 9780727725844.
- [87] T. M. Karlsson, L. Arneborg, G. Broström, B. C. Almroth, L. Gipperth, and M. Hassellöv, "The unaccountability case of plastic pellet pollution," *Marine Pollution Bulletin*, vol. 129, no. 1, pp. 52–60, 2018.

[88] T. M. Karlsson, L. Arneborg, G. Broström, B. C. Almroth, L. Gipperth, and M. Hassellöv, "The unaccountability case of plastic pellet pollution," *Marine Pollution Bulletin*, vol. 129, no. 1, pp. 52–60, 2018.